Modification of Excited State Behavior with Ligand Substitution in Ru(II),Rh(III) Bimetallic Supramolecular Complexes

Hannah J. Sayre

Thesis submitted to the faculty of the Virginia Polytechnic Institute and State University
in partial fulfillment of the requirements for the degree of

Master of Science
In
Chemistry

James M. Tanko (Chair)
Karen J. Brewer (Co-Chair)
Amanda J. Morris
Paul A. Deck

May 11, 2015
Blacksburg, VA

Keywords: supramolecule, photochemistry, electron-withdrawing, excited state lifetime, water reduction

Modification of Excited State Behavior with Ligand Substitution in Ru(II),Rh(III) Bimetallic Supramolecular Complexes

Hannah J. Sayre

Abstract

The terminal ligand in $[(Ph_2phen)_2Ru(dpp)RhCl_2(TL)](PF_6)_3$ (Ph_2phen = 4,7-diphenyl-1,10-phenanthroline; dpp = 2,3-bis(2-pyridyl)pyrazine; TL = terminal ligand – a 4,4′-di-substituted-2,2′-bipyridine where the substituent was carbomethoxy (dcmbpy), hydrogen (bpy) or methyl (Me_2bpy)). The electron-withdrawing ability of the substituent was shown to increase the rate of chloride loss upon electrochemical reduction, facilitating catalytic water reduction. The electronic properties of the terminal ligand also impact the photophysical properties of the molecule. The excited state lifetime of the complex with a dcmbpy terminal ligand was 93 ns while the excited state lifetimes of the complexes with a bpy or Me_2bpy terminal ligand were 44 ns and 47 ns, respectively. Ligand substitution was shown to influence the photocatalytic water reduction activity of these complexes with the dcmbpy complex producing approximately twice the amount of hydrogen (62 ± 7 turnovers in 20 h) as the other two complexes.

Acknowledgements

I am forever thankful for the time spent at Virginia Tech with my colleagues, my advisors, committee members and family. I am honored to have worked for Dr. Karen Brewer and appreciate everything I learned from her. I will never put electrons in a state diagram or arrows in an orbital diagram. She taught me the importance of sharing science with the community and increasing diversity in research. Members of the Brewer Group have been both supportive and challenging and have become part of my extended family. I am especially grateful to Theodor Canterbury, Hannah Rogers and Alec Wagner for help with research discussions, equipment maintenance and writing development. I am thankful for help with electrochemistry experiments from Marwa Abdel Latif. I am immensely grateful for my spouse, Spencer Dennis, who has been tremendously encouraging, has sacrificed a portion of his career and worked additional hours to help take care of our two children. I appreciate our children and the difficult questions they ask. I am thankful for my father, Steve Sayre, who instilled in me a love of learning at an early age. My committee members, Dr. James Tanko, Dr. Amanda Morris, and Dr. Paul Deck, have contributed significantly to my education. They have been extraordinarily helpful in the past year, especially. I am very grateful to Dr. James Tanko for stepping in as my committee chair and for his guidance with electrochemistry. Dr. Amanda Morris and Dr. Paul Deck both invested significant thought and time in asking thoughtful and insightful questions. I am additionally thankful to Dr. Deck for teaching me how to teach. I express gratitude to the U.S. Department of Energy for research funding.

Table of Contents

List of Figures

photochemically (**A**) and electrochemically (**B**) in acetonitrile. This image is copied from reference 7d.

Figure 1.12: Cyclic voltammetry in 0.1 M Bu_4NPF_6/CH_3CN of $[(phen)_2Ru(dpp)RhCl_2(bpy)](PF_6)_3$ before (**a**) and after bulk electrolysis at −0.60 V in an H-cell (**b**) (phen = 1,10-phenanthroline; dpp = 2,3-bis(2-pyridyl)pyrazine; bpy = 2,2′-bipyridine). This image is copied from reference 7d, supporting information.

Figure 1.13: Cyclic voltammograms of $[(Ph_2phen)_2Ru(dpp)RhBr_2(Ph_2phen)](PF_6)_3$ (blue), $[(Ph_2phen)_2Ru(dpp)RhCl_2(Ph_2phen)](PF_6)_3$ (green) and $[(Ph_2phen)_2Ru(dpp)RhBr_2(^tBu_2bpy)](PF_6)_3$ (red) with 0.1 M Bu_4NPF_6 in CH_3CN supporting electrolyte. The scan rate applied was 100 $mV \cdot s^{-1}$. This image is copied from reference 7g.

Figure 1.14: Ratio of the second cathodic peak current to the first cathodic peak current vs. the square root of scan rate for $[(Ph_2phen)_2Ru(dpp)RhCl_2(^tBu_2bpy)](PF_6)_3$ (red diamonds), $[(Ph_2phen)_2Ru(dpp)RhCl_2(Ph_2phen)](PF_6)_3$ (green squares) and $[(Ph_2phen_2Ru(dpp)RhBr_2(Ph_2phen)](PF_6)_3$ (blue circles) with 0.1 M Bu_4NPF_6 in CH_3CN supporting electrolyte. This image is copied from reference 7g.

Figure 1.15: Chemical structures of the bimetallic complexes $[(Ph_2phen)_2Ru(dpp)RhCl_2(Me_2bpy)](PF_6)_3$, $[(Ph_2phen)_2Ru(dpp)RhCl_2(bpy)](PF_6)_3$ and $[(Ph_2phen)_2Ru(dpp)RhCl_2(dcmbpy)](PF_6)_3$ (Ph_2phen = 4,7-diphenyl-1,10-phenanthroline; dpp = 2,3-bis(2-pyridyl)pyrazine; Me_2bpy = 4,4′-dimethyl-2,2′-bipyridine; bpy = 2,2′-bipyridine; dcmbpy = 4,4′-dicarbomethoxy-2,2′-bipyridine).

Figure 2.1: Correction factor for PMT response in the 500 to 1000 nm wavelength range.

Figure 3.1: Synthetic scheme for $[(Ph_2phen)_2Ru(dpp)RhCl_2(R_2bpy)](PF_6)_3$ (Ph_2phen = 4,7-diphenyl-1,10-phenanthroline; dpp = 2,3-bis(2-pyridyl)pyrazine; R_2bpy = 4,4′-disubstituted-2,2′-bipyridine where the substituent is CH_3, H or $COOCH_3$.

Figure 3.2: Cyclic voltammograms of $[(Ph_2phen)_2Ru(dpp)RhCl_2(Me_2bpy)](PF_6)_3$ (orange), $[(Ph_2phen)_2Ru(dpp)RhCl_2(bpy)](PF_6)_3$ (green) and $[(Ph_2phen)_2Ru(dpp)RhCl_2(dcmbpy)](PF_6)_3$ (purple) with 0.1 M Bu_4NPF_6/CH_3CN supporting electrolyte and a 100 mV/s applied scan rate.

Figure 3.3: Ratio of anodic to cathodic peak current vs. scan rate. Variable scan rate cyclic voltammograms of $[(Ph_2phen)_2Ru(dpp)RhCl_2(Me_2bpy)](PF_6)_3$ (orange triangles), $[(Ph_2phen)_2Ru(dpp)RhCl_2(bpy)](PF_6)_3$ (green circles) and $[(Ph_2phen)_2Ru(dpp)RhCl_2(dcmbpy)](PF_6)_3$ (purple squares) with a glassy carbon working electrode, Pt wire auxiliary, and Ag/AgCl reference in 0.1 M Bu_4NPF_6/CH_3CN supporting electrolyte. Potential sweeps were applied with a BAS potentiostat.

Figure 3.4: DigiSim models (dashed lines) overlaid with experimental CVs (solid lines) for $[(Ph_2phen)_2Ru(dpp)RhCl_2(Me_2bpy)](PF_6)_3$ (orange) and $[(Ph_2phen)_2Ru(dpp)RhCl_2(dcmbpy)](PF_6)_3$ (purple). Experimental CVs were obtained with a 0.1 M Bu_4NPF_6/CH_3CN supporting electrolyte. A potential sweep of 100 mV/s was applied with a BAS potentiostat.

Figure 3.5: Variable scan rate cyclic voltammograms of $[(Ph_2phen)_2Ru(dpp)RhCl_2(Me_2bpy)](PF_6)_3$ (**a**), $[(Ph_2phen)_2Ru(dpp)RhCl_2(bpy)](PF_6)_3$ (**b**) and $[(Ph_2phen)_2Ru(dpp)RhCl_2(dcmbpy)](PF_6)_3$ (**c**) with a glassy carbon working electrode, Pt wire auxiliary, and Ag/AgCl reference in 0.1 M Bu_4NPF_6/CH_3CN supporting electrolyte. A PAR potentiostat with iR compensation was used. CVs shown had an applied scan rate of 100 (purple), 500 (blue), 900 (green), 1500 (orange) and 2000 (red) $mV \cdot s^{-1}$.

Figure 3.6: Peak current ratio $i_p^{c}{}_{(II)}/i_p^{c}{}_{(I)}$ vs. scan rate for $[(Ph_2phen)_2Ru(dpp)RhCl_2(Me_2bpy)](PF_6)_3$ (orange triangles), $[(Ph_2phen)_2Ru(dpp)RhCl_2(bpy)](PF_6)_3$ (green circles) and $[(Ph_2phen)_2Ru(dpp)RhCl_2(dcmbpy)](PF_6)_3$ (purple squares). A PAR potentiostat with iR compensation was used to apply 100, 300, 500, 700, 900, 1200, 1500, 1700, 2000, 2500 and 2800 $mV \cdot s^{-1}$ scan rates.

Figure 3.7: Electronic absorption spectra of $[(Ph_2phen)_2Ru(dpp)RhCl_2(Me_2bpy)](PF_6)_3$, $[(Ph_2phen)_2Ru(dpp)RhCl_2(bpy)](PF_6)_3$ and $[(Ph_2phen)_2Ru(dpp)RhCl_2(dcmbpy)](PF_6)_3$ in spectrophotometric grade acetonitrile.

Figure 3.8: Steady-state emission spectra of $[(Ph_2phen)_2Ru(dpp)RhCl_2(Me_2bpy)](PF_6)_3$ (orange), $[(Ph_2phen)_2Ru(dpp)RhCl_2(bpy)](PF_6)_3$ (green), $[(Ph_2phen)_2Ru(dpp)RhCl_2(dcmbpy)](PF_6)_3$ (purple) collected at room temperature in deaerated spectrophotometric grade acetonitrile.

Figure 3.9: Photocatalytically produced hydrogen with $[(Ph_2phen)_2Ru(dpp)RhCl_2(dcmbpy)](PF_6)_3$ (purple squares), $[(Ph_2phen)_2Ru(dpp)RhCl_2(bpy)](PF_6)_3$ (green circles) and $[(Ph_2phen)_2Ru(dpp)RhCl_2(Me_2bpy)](PF_6)_3$ (orange triangles) in DMF. Total solution volume was 4.5 mL (130 μmol catalyst, 0.62 M H_2O, 1.5 M DMA, 0.11 mM $[DMA^+][CF_3SO_3^-]$) and 15.5 mL headspace.

Figure A.1: Mass spectrum molecular ion peak of $(dcmbpy)RhCl_3 \cdot DMF$.

Figure A.2: Mass spectrum of $[(Ph_2phen)_2Ru(dpp)RhCl_2(Me_2bpy)](PF_6)_3$. Molecular ion peak is $[[(Ph_2phen)_2Ru(dpp)RhCl_2(Me_2bpy)](PF_6)_2]^+$.

Figure A.3: Mass spectrum of $[(Ph_2phen)_2Ru(dpp)RhCl_2(bpy)](PF_6)_3$. Molecular ion peak is $[[(Ph_2phen)_2Ru(dpp)RhCl_2(bpy)](PF_6)_2]^+$.

List of Tables

1. Introduction

1.1. Solar Energy

Development of alternative energy sources is essential to meet the rising global energy demand. Fossil fuels do not provide a sustainable source of energy due to their limited supply and their impact on climate change. Solar energy offers a plausible solution to the energy crisis. Worldwide energy consumption in 2010 was less than 0.02% of the potential energy reaching the earth's surface in one year.[1]

Capturing and storing solar energy are the primary difficulties associated with making solar energy competitive with fossil fuels.[1a] Systems capable of capturing energy from sunlight and converting it to usable fuel are therefore of great interest.[1a,2] Photocatalytic reduction of water to produce molecular hydrogen provides a means to capture solar energy and store that energy as a high-density fuel.

Photocatalytic water reduction requires light absorption, electron relay, an electron source and an active catalytic site. Most of the energy from light striking the earth's surface is in the visible range of the solar spectrum (**Figure 1.1**).[3] Since water does not absorb visible light, a light absorber is necessary to capture the energy from light. The excited light absorber promotes an electron into an electron relay, which transfers an electron to the active catalytic site.

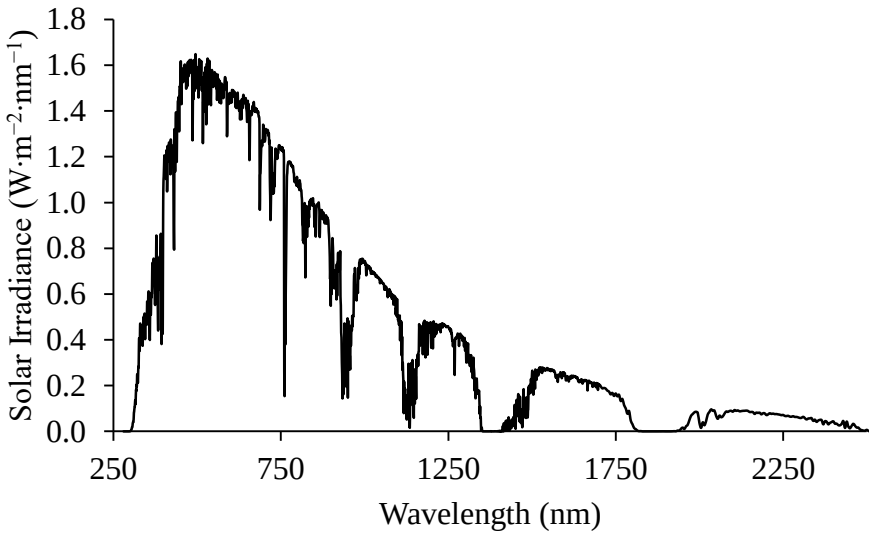

Figure 1.1: Solar energy power at the earth's surface per square meter for each wavelength.

The first Ru(II),Rh(III) system developed to reduce water photocatalytically used multiple components to capture energy from light, excite an electron into an excited state and relay the electron to an active catalyst.[4] This system required a light absorber, an electron donor, an electron relay and an electron collector (**Figure 1.2**). Intermolecular electron transfer in multicomponent systems requires molecular interaction among all the components in solution. The rate of diffusion limits overall efficiency so relatively high concentrations are required. The concentration requirements of multicomponent systems are undesirable due to the expensive and sparingly soluble components.

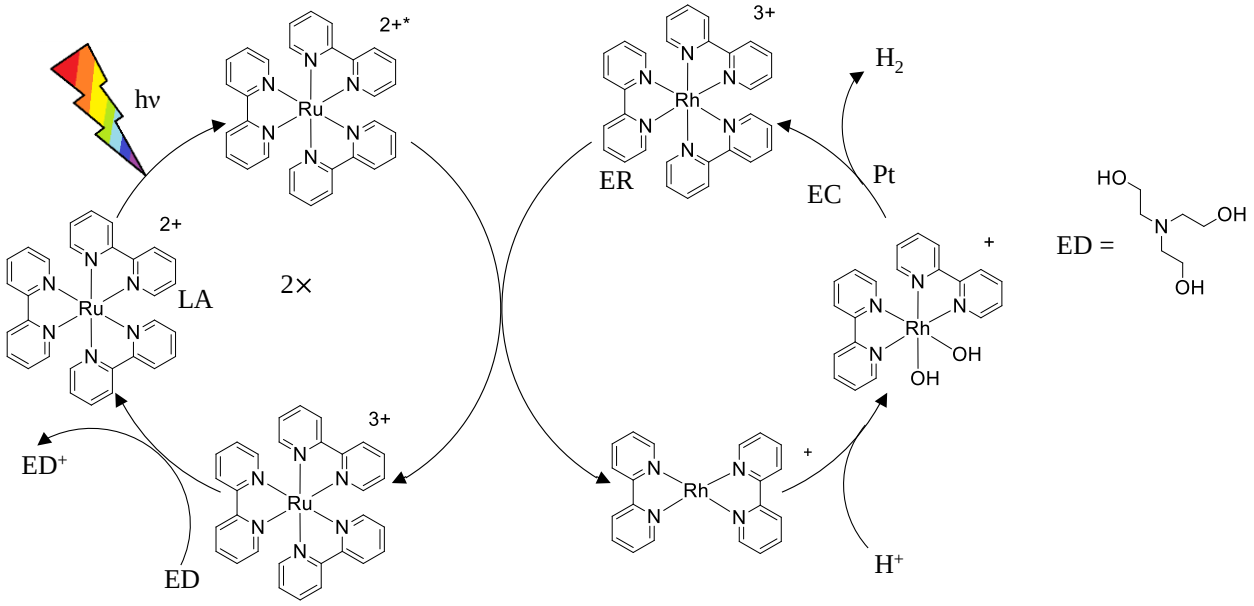

Figure 1.2: Catalytic mechanism for the first reported multicomponent system for photocatalytic water reduction. The LA is $[Ru(bpy)_3]^{2+}$ (bpy = 2,2′-bipyridine), ED is triethanolamine , ER is $[Rh(bpy)_3]^{3+}$ and EC is colloidal Pt. This mechanism is reported in reference 2.

1.2. Supramolecular Chemistry

Supramolecular complexes covalently bind multiple components while maintaining the unique function of each component.[5] Electron transfer in supramolecular complexes occurs intramolecularly, which permits lower concentrations. Many supramolecular motifs have been reported which absorb light and transfer energy or electrons.[6] The Brewer Group has studied many supramolecular photocatalysts for water reduction in which the light absorber and active catalytic site are covalently connected through a bridging ligand (**Figure 1.3**).[7]

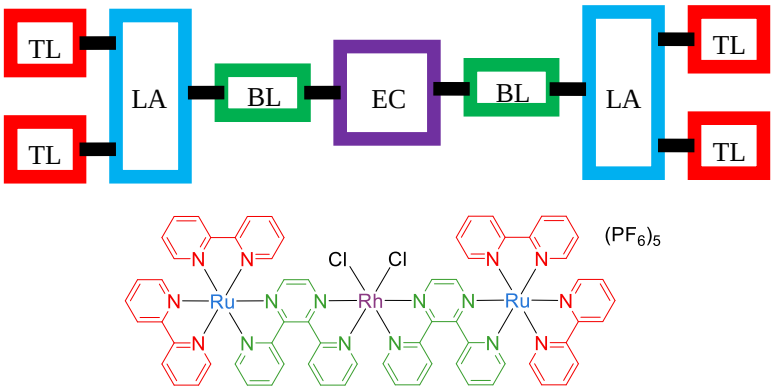

Figure 1.2: Block diagram of a supramolecule (TL = terminal ligand; LA = light absorber; BL = bridging ligand) and a supramolecular photocatalyst $[\{(bpy)_2Ru(dpp)\}_2RhCl_2](PF_6)_5$ (bpy = 2,2′-bipyridine; dpp = 2,3-bis(2-pyridyl)pyrazine).

1.3. Photochemistry

Ru polypyridyl light absorbers have promising solar energy applications.[7c,8] Upon absorption of light, Ru polypyridyl complexes promote an electron from a Ru-based molecular orbital (MO) into a ligand-based MO, generating a metal-to-ligand charge transfer (^{1}MLCT) excited state.[6,9] The electron undergoes intersystem crossing to populate the ^{3}MLCT excited state at near unit efficiency.[10]

Population of a ^{1}MLCT excited state upon light absorption and unit population of ^{3}MLCT excited state is also observed in the supramolecular complexes reported by Brewer.[11] Excitation by light results in multiple paths of relaxation. Radiative decay from the ^{3}MLCT excited state back to the ground state is observed as phosphorescent emission and is catalytically unproductive. Non-radiative decay processes from the ^{3}MLCT and ^{3}MMCT excited states back to the ground state are also competing, unproductive processes (**Figure 1.4**).

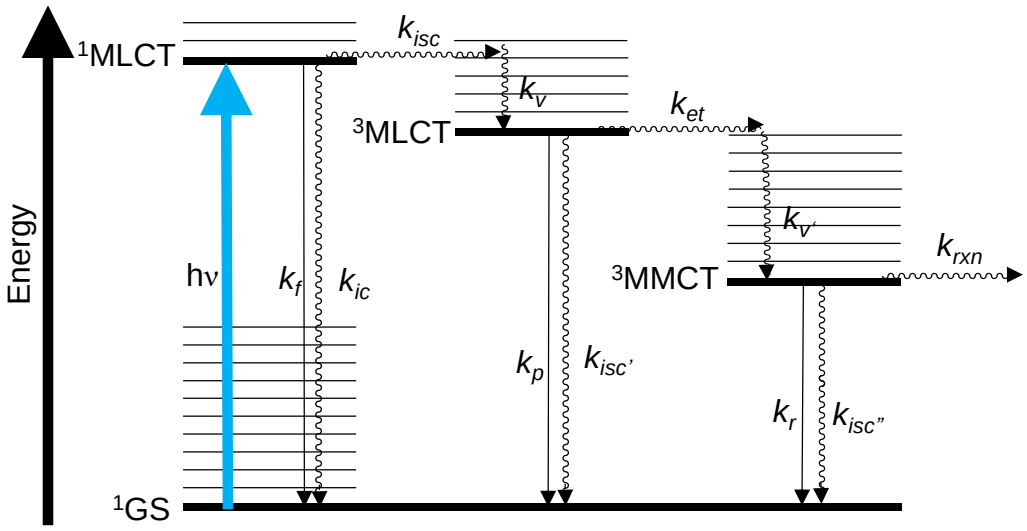

Figure 1.3: State diagram depicting photoexcitation of a supramolecular photocatalyst and the multiple forms of relaxation (hν = photoexcitation; k_f = rate constant for fluorescence; k_{ic} = rate constant for internal conversion; k_{isc} = rate constant for intersystem crossing; k_v = rate constant for vibronic relaxation; k_p = rate constant for phosphorescence; k_{et} = rate constant for electron transfer; k_r = rate constant for radiative decay; k_{rxn} = rate constant for reaction; radiative decay processes are depicted as ——— ; non-radiative decay processes are depicted as ∿∿∿).

The most active supramolecular photocatalysts have excited state energy levels that optimize energy flow from the ^{1}MLCT excited state to populate a metal-to-metal charge transfer (^{3}MMCT) excited state.[7a,7b] Complexes with a bridging ligand-based LUMO prevent electron flow to Rh.[7b,7g,12] An additional consideration is the energy level of the ^{3}MLCT excited state relative to the reduction potential of the sacrificial electron donor. Water reduction with these photocatalysts requires sufficient driving force for quenching of the ^{3}MLCT excited state by the electron donor.[7b] The ultimate goal of this type of research is to couple photocatalytic water reduction with water oxidation, obviating the sacrificial electron donor, but that is beyond the scope of this discussion.

Structural modifications that either stabilize the unoccupied Rh e_g* orbitals or destabilize the bridging ligand are of interest since the bridging ligand-based and Rh-based unoccupied orbitals are close in energy.[7b] Both Rh stabilization and bridging ligand destabilization result in an increased energy gap between the ^{3}MLCT and ^{3}MMCT excited states, increasing the driving force to populate the ^{3}MMCT excited state.

One method to stabilize unoccupied Rh orbitals is to decrease the σ-donating ability of coordinated halide. The $Rh^{III/II/I}$ reduction potential in $[Rh(bpy)_2X_2]^+$ complexes shifts to more positive potential as the σ-donating ability of the coordinated halide decreases (**Figure 1.5**).[13] The Δ_o is smallest when iodide is coordinated to Rh and increases as halide size decreases.

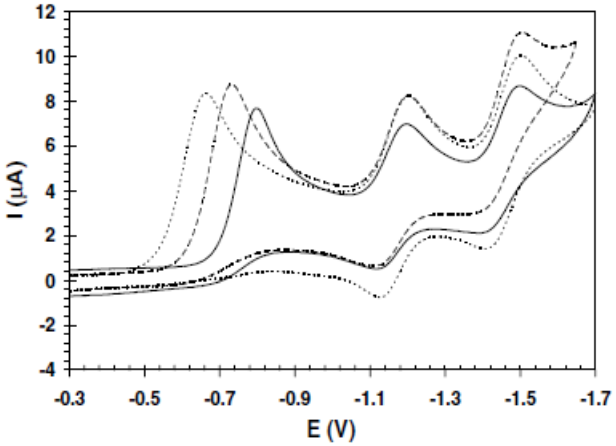

Figure 1.5: Cyclic voltammograms of $[Rh(bpy)_2X_2]^+$ in 0.1 M Bu_4NPF_6/DMF with Ag/AgCl reference electrode at room temperature. The scan rate applied was 100 $mV \cdot s^{-1}$. Coordinated halide, X = Cl (—), Br (- - ·), I (·····). This image is copied from reference 13.

The energy level of the ^{3}MMCT excited state relative to the reduction potentials of water and of the ^{3}MLCT excited state are important for the rate of water reduction based on Marcus theory.[14] The Eyring equation (**eq. 1.1**) shows that outside of the Marcus inverted region, k_{et} increases with increasing energy gap.[15] The frequency factor is Z, $\Delta G^{\ddagger}$ is the free energy of activation, R is the ideal gas constant and T is temperature. Outside the Marcus inverted region, k_{et} increases as the energy gap between the ^{3}MLCT excited state and ^{3}MMCT excited state reduction potentials expands.

$$k_{et} = Z\, e^{-\Delta G^{\ddagger}/RT} \qquad \textbf{(1.1)}$$

1.4. Methods

Several analytical methods are required to investigate the relative energy levels of molecular orbitals and the relative energies of excited states. Electronic absorption spectroscopy and emission spectroscopy provide the excited state energies of the ^{1}MLCT and ^{3}MLCT excited states, respectively, relative to the ground state. The ^{1}MLCT excited state energy is approximately equal to the energy gap between the metal-based MO and the ligand-based MO. Cyclic voltammetry provides the ground state energy gap between the highest occupied molecular orbital (HOMO) and the LUMO. To gain a complete picture of orbital energetics and excited state reactions, electrochemical and photophysical data must be considered together.

Emission spectroscopy measures the radiative decay of an excited state. Fluorescence, which is radiative decay from a singlet excited state, is not observed due to immediate and quantitative intersystem crossing to population of the ^{3}MLCT state.[16] Radiative decay is observed after the electron undergoes a spin flip to populate the ^{3}MLCT excited state. An approximation of the ^{3}MLCT energy level is obtained from the wavelength of room temperature phosphorescence but vibronic relaxation interferes with obtaining the reduction potential of the ^{3}MLCT excited state at room temperature. The ^{3}MLCT excited state energy level relative to the ground state (E_{00}) is obtained by measuring the emission at 77 K. The reduction potential of the ^{3}MLCT excited state ($Ru^{3+/2+}(LL^{-})$ in **Figure 1.6**) is calculated using the E_{00} from 77 K emission and the reduction potential of the ligand (**eq. 1.2** and 1.**3**).[17] This method is somewhat limited due to possible inaccuracies in the ligand reduction potentials, which will be discussed in more detail later.

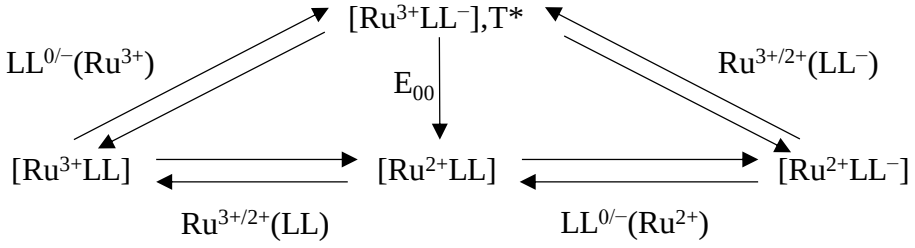

Figure 1.6: Scheme for determining the reduction potential of the ^{3}MLCT excited state. This image is adapted from reference 17.

$$E\left(LL^{0/-}(Ru^{3+})\right) = E\left(Ru^{3+/2+}(LL)\right) - E_{00} \quad \textbf{(1.2)}$$

$$E\left(Ru^{3+/2+}(LL^{-})\right) = E\left(LL^{0/-}(Ru^{2+})\right) + E_{00} \quad \textbf{(1.3)}$$

Room temperature emission quantum yield (Φ^{em}) is the ratio of radiative decay to the sum of all deactivation pathways from the ^{3}MLCT excited state (**eq. 1.4**). Quantum yield of population (Φ_{pop}) is assumed to be unity. Lower emission quantum yields indicate more efficient quenching by the ^{3}MMCT excited state and a greater rate constant for electron transfer (k_{et}).

$$\Phi^{em} = \Phi^{pop}_{^3MLCT} \frac{k_r}{k_r + k_{nr} + k_{et}} \quad \textbf{(1.4)}$$

Time-resolved emission spectroscopy is a pulsed laser technique that measures the decay of emission from the ^{3}MLCT excited state over time. The lifetime (τ) of an excited state is the inverse of the sum of all forms of relaxation from the excited state (**eq. 1.5**). The k_{et} is determined by comparing the observed lifetime to that of a model complex in which electron transfer from the ^{3}MLCT excited state to the ^{3}MMCT excited state does not occur (**eq. 1.6**). A Ru-Ru bimetallic with the same bridging and terminal ligands as the molecule of interest is typically used as the model (**Figure 1.7**). It is assumed that k_r and k_{nr} remain constant.

$$\tau = \frac{1}{k_r + k_{nr} + k_{et}} \quad \textbf{(1.5)}$$

$$\tau_{model} = \frac{1}{k_r + k_{nr}} \quad \textbf{(1.6)}$$

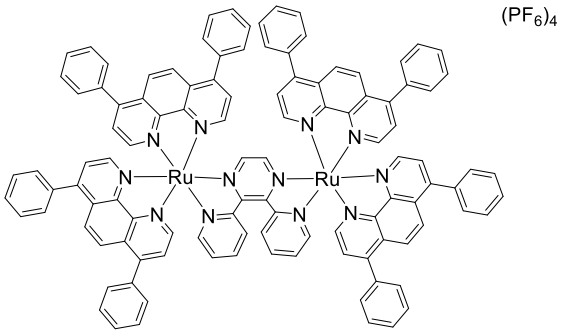

Figure 1.7: An example of a Ru-Ru bimetallic model, $[\{(Ph_2phen)_2Ru\}_2dpp](PF_6)_4$ (Ph_2phen = 4,7-diphenyl-1,10-phenanthroline; dpp = 2,3-bis(2-pyridyl)pyrazine).

Cyclic voltammetry (CV) is a potential sweep method used to determine the relative orbital energetics of the studied species in the ground state. The ground state energy level of the HOMO is assigned to the first anodic couple E°. The E° of the first cathodic couple is assigned to the ground state energy level of the LUMO.

CV is limited to providing the relative energies of the HOMO and LUMO only. Oxidation of the HOMO and reduction of the LUMO alters the orbital energetics, making any E° past the HOMO and LUMO an inaccurate description of orbital energetics. The LUMO in many of Brewer's supramolecules resides primarily on Rh rather than on the ligand. The calculation of the ^{3}MLCT excited state reduction potential (**eq. 1.3**) is limited since an accurate E° of the ligand can only be obtained if the LUMO is ligand-based.

Variable scan rate CV is used to identify reversible electrochemical processes and study non-reversible electrochemical processes.[18] Non-reversibility of a redox couple indicates a chemical reaction following the electrochemical reaction. Reversibility of the couple increases with increasing scan rate if the chemical reaction occurs on the CV time scale.

The nature of the LUMO – whether it is predominantly bridging ligand-based or Rh-based – is determined by the reversibility of the first cathodic current. Non-reversibility of a cathodic couple indicates an irreversible chemical reaction following reduction. Reduction of a Rh-based orbital is expected to result in chloride loss due to a decrease in bond order. The rate of a follow-up chemical reaction might be determined if it can be matched by the potential scan rate. Variation of scan rates is necessary to determine

reversibility of reduction couples and has been used to determine the nature of the LUMO and provide mechanistic insight into catalysis.[7g,19]

1.5. Ligand Effects on Rhodium Reduction in Rh Polypyridyl Complexes

The general effects of σ-donating, π-donating and π-accepting ligands on molecular orbitals of octahedral metal complexes are fairly well understood.[20] The orbital overlap between metal-based orbitals and ligand-based orbitals affects the energy levels of the combined molecular orbitals. Light-activated reactions and catalysis are impacted by minute changes in orbital energetics.

A ligand's σ-donating ability strongly influences orbital energetics of octahedral d^6 metal complexes. Ligands that have more orbital overlap with the metal are better σ-donors and stabilize the e_g bonding orbital (**Figure 1.8**). Simultaneous destabilization of the antibonding e_g* occurs with stabilization of the bonding e_g MO and increases Δ_o, the energy gap between the t_{2g} and e_g* MOs.

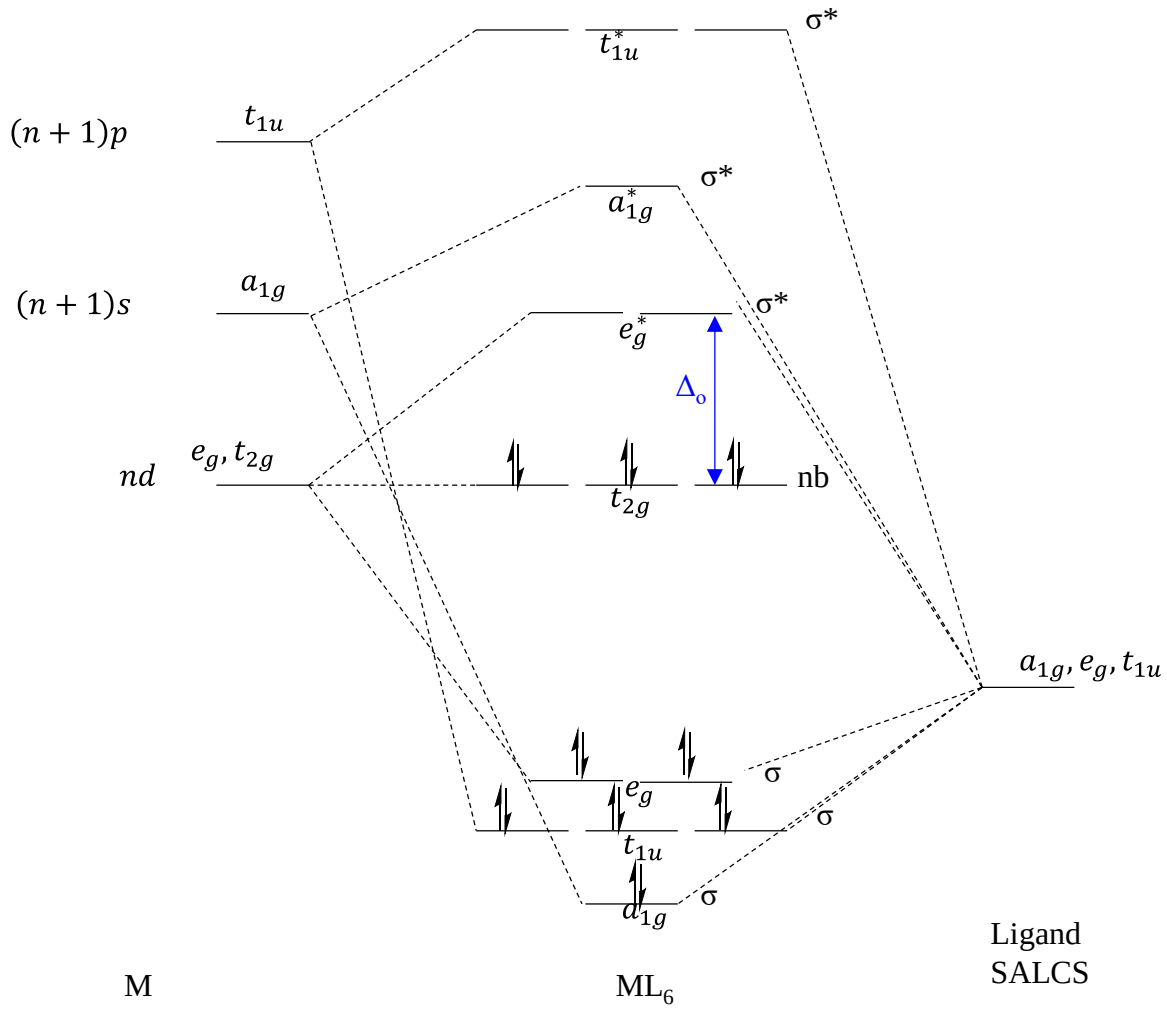

Figure 1.8: Molecular orbital diagram of a d^6 octahedral metal complex with σ-donating ligands. This image is adapted from reference 20.

The electrochemical analysis of Rh polypyridyl complexes by DeArmond in the 1970s provides a foundation for studying the orbital energetics of Rh supramolecular photocatalysts. The LUMO in both $[Rh(bpy)_2Cl_2]^+$ and $Rh(phen)_2Cl_2]^+$ (bpy = 2,2′-bipyridine; phen = 4,7-phenanthroline) is Rh-based and the first cathodic couple is irreversible even at scan rates as fast as 32 $V \cdot s^{-1}$.[21] Halide loss is rapid upon $Rh^{III/II/I}$ reduction. There are two independent ligand reductions, indicating electronic communication between polypyridyl ligands.[21] Although phen is reduced at a more positive potential than bpy, the $Rh^{III/II/I}$ $E_{1/2}$ is consistent in $[Rh(bpy)_2Cl_2]^+$ and $Rh(phen)_2Cl_2]^+$.[21]

The energy of the ligand field excited state in rhodium polypyridyl dibromide complexes decreases as the electronegativity of the reduction of the polypyridyl ligand shifts more positive (**Figure 1.9**, **Table 1.1**).[11] Increased electronegativity of the ligand stabilizes the ligand field excited state. Stabilization of the ligand field excited state in low-spin d^6 metals coincides with stabilization of e_g* MOs.

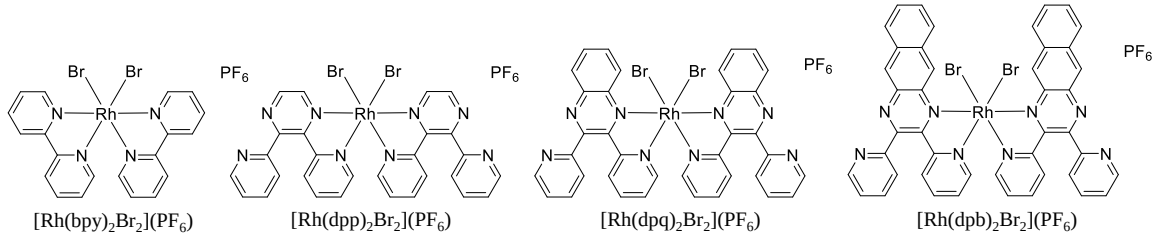

Figure 1.9: Rhodium polypyridyl complexes with two coordinated bromides (bpy = 2,2′-bipyridine; dpp = 2,3-bis(2-pyridyl)pyrazine; dpq = 2,3-bis(2-pyridyl)quinoxaline; dpb = 2,3-bis(2-pyridyl)benzoquinoxaline).

Table 1.1: Ligand reduction (referenced to Ag/AgCl) and ligand field 77 K emission wavelengths of rhodium polypyridyl dibromide complexes as reported in reference 11.

Complex	**$E_{1/2}$ (V vs. Ag/AgCl)**	**λ^{em} (nm)**
$[Rh(bpy)_2Br_2]^+$	−1.30 −1.50	660
$[Rh(dpp)_2Br_2]^+$	−1.05 −1.19	707
$[Rh(dpq)_2Br_2]^+$	−0.85 −1.49	737
$[Rh(dpb)_2Br_2]^+$	−0.39	N/A[a]

[a] Emission could not be detected due to the low red detection of the photomultiplier tube.

1.6. Ru(II),Rh(III) Bimetallic Complexes for Photocatalysis

The Brewer Group has investigated variations in the halide and the terminal ligand on Rh (**Figure 1.10**).[7d,7f-h] A correlation exists between the σ-donating ability of the halide and the rate of halide loss which is a significant step in the catalytic mechanism of these molecules.[7g] The terminal ligand on Rh also plays an important role in the catalytic ability of the bimetallic to reduce water.[7d,7g,7h] Consideration of the steric and electronic

characteristics of the terminal ligand are crucial in the development of active bimetallic photocatalysts.[7h]

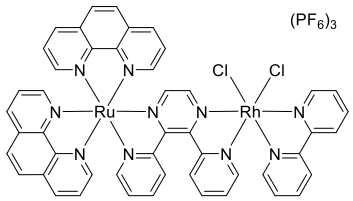

$[(phen)_2Ru(dpp)RhCl_2(bpy)](PF_6)_3$

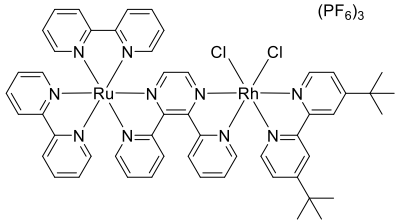

$[(bpy)_2Ru(dpp)RhCl_2(^tBu_2bpy)](PF_6)_3$

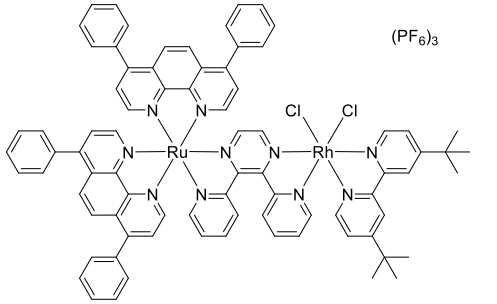

$[(Ph_2phen)_2Ru(dpp)RhCl_2(^tBu_2bpy)](PF_6)_3$

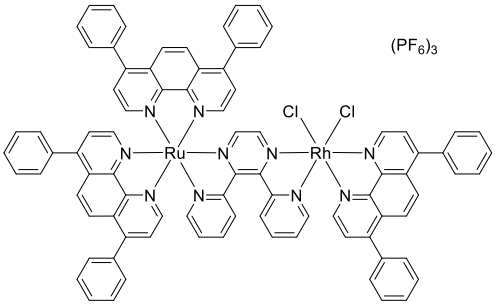

$[(Ph_2phen)_2Ru(dpp)RhCl_2(Ph_2phen)](PF_6)_3$

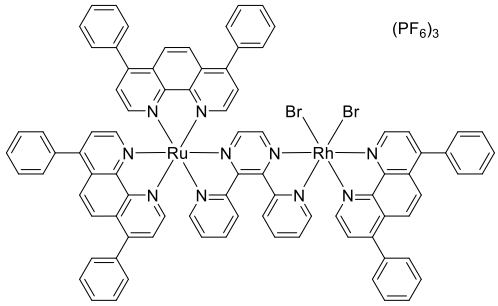

$[(Ph_2phen)_2Ru(dpp)RhBr_2(Ph_2phen)](PF_6)_3$

Figure 1.10: Previously published Ru(II),Rh(III) bimetallic complexes analyzed for H_2O reduction in the Brewer group (phen = 1,10-phenanthroline; dpp = 2,3-bis(2-pyridyl)pyrazine; bpy = 2,2′-bipyridine; $^tBu_2bpy$ = 4,4′-di-*tert*-butyl-2,2′-bipyridine; Ph_2phen = 4,7-diphenyl-1,10-phenanthroline).

The first Ru(II),Rh(III) bimetallic analyzed for H_2 production by Brewer was $[(phen)_2Ru(dpp)RhCl_2(bpy)](PF_6)_3$ (**Figure 1.10**).[7d] The bimetallic $[(phen)_2Ru(dpp)RhCl_2(bpy)](PF_6)_3$ absorbs light and transfers an electron to Rh. Electronic absorption spectra during photo-reduction and electrochemical reduction are nearly identical (**Figure 1.11**).[7d] Cyclic voltammetry shows the first cathodic reduction

current is non-reversible, indicating that the LUMO is Rh-based, with halide loss upon Rh reduction (**Figure 1.12a**).[7d] Most of the photochemical and electrochemical data indicate that $[(phen)_2Ru(dpp)RhCl_2(bpy)](PF_6)_3$ should act as an active photocatalyst for water reduction. The first cathodic couple is non-reversible, indicating halide loss upon Rh reduction.

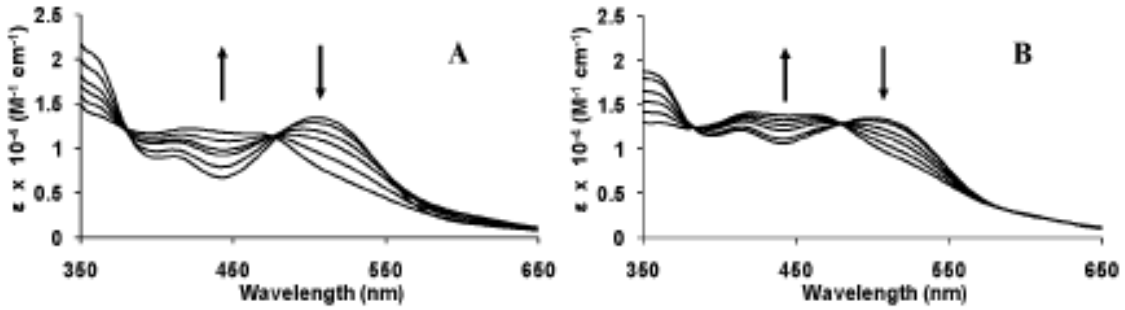

Figure 1.11: Electronic absorption spectroscopic changes resulting from reduction of $[(phen)_2Ru(dpp)Rh^{III}Cl_2(bpy)](PF_6)_3$ to $[(phen)_2Ru(dpp)Rh^{I}Cl_2(bpy)](PF_6)$ photochemically (**A**) and electrochemically (**B**) in acetonitrile. This image is copied from reference 7d.

Although the photochemical and electrochemical reductions suggest a successful photocatalyst, the bimetallic forms a Rh-Rh dimer upon Rh reduction. Bulk electrolysis at −0.60 V immediately followed by mass spectrometry provides evidence of dimerization with a molecular ion peak of the Rh-Rh dimer and several fragments of the dimer.[7d] Cyclic voltammetry prior to bulk electrolysis shows one reversible Ru oxidation with E° = 1.6 V vs. Ag/AgCl (**Figure 1.12a**).[7d] A cyclic voltammogram following bulk electrolysis shows an additional oxidation with E° = 1.0 V vs. Ag/AgCl, indicating the presence of a new Ru species (**Figure 1.12b**). The lack of photocatalytic activity by $[(phen)_2Ru(dpp)RhCl_2(bpy)](PF_6)_3$ to reduce water is attributed to the dimerization at Rh.[7d] The bpy ligand does not provide significant steric hindrance to prevent Rh-Rh dimerization.

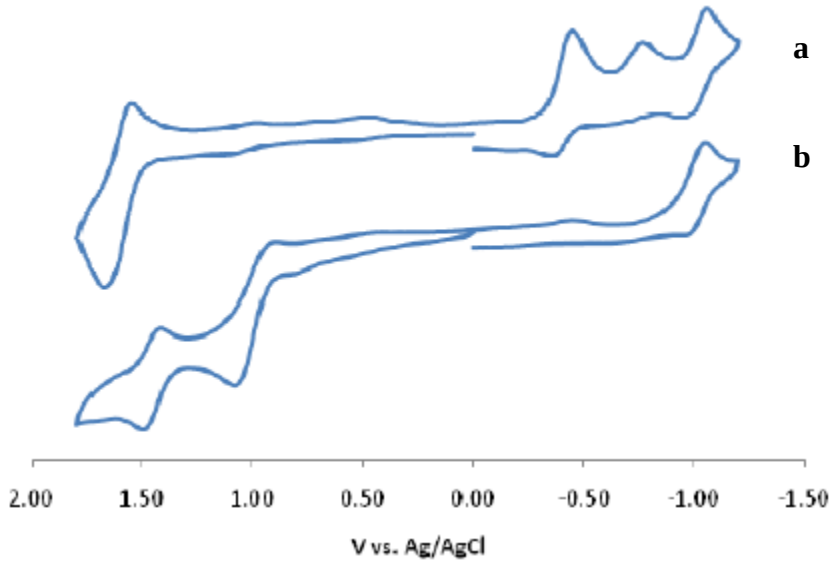

Figure 1.12: Cyclic voltammetry in 0.1 M Bu_4NPF_6/CH_3CN of $[(phen)_2Ru(dpp)RhCl_2(bpy)](PF_6)_3$ before (**a**) and after bulk electrolysis at −0.60 V in an H-cell (**b**) (phen = 1,10-phenanthroline; dpp = 2,3-bis(2-pyridyl)pyrazine; bpy = 2,2′-bipyridine). This image is copied from reference 7d, supporting information.

Evidence of dimer formation led to incorporation of more sterically bulky terminal ligands on Rh. Two bimetallic complexes with sterically bulky terminal ligands, $[(bpy)_2Ru(dpp)RhCl_2(^tBu_2bpy)](PF_6)_3$ and $[(Ph_2phen)_2Ru(dpp)RhCl_2(Ph_2phen)](PF_6)_3$, were analyzed for photocatalytic activity.[7h] Although both bimetallic complexes have sterically bulky terminal ligands, only $[(Ph_2phen)_2Ru(dpp)RhCl_2(Ph_2phen)](PF_6)_3$ is an active photocatalyst for water reduction.[7h] The inability of $[(bpy)_2Ru(dpp)RhCl_2(^tBu_2bpy)](PF_6)_3$ to produce hydrogen was attributed to the electron-donating ability of the *tert*-butyl substituent.[7h] However, it is known that $[(Ph_2phen)_2Ru(dpp)](PF_6)_2$ light absorbers coordinated to Rh are better photocatalysts than $[(bpy)_2Ru(dpp)](PF_6)_2$ and the difference in water reducing ability is likely due in part to variation of the light absorbing unit.[7c]

The σ-donating ability of ligands plays an important role in the catalytic activity of these supramolecules. The $[(Ph_2phen)_2Ru(dpp)RhCl_2(Ph_2phen)](PF_6)_3$ bimetallic complex produces molecular hydrogen at about half the rate of the analogous $[\{(Ph_2phen)_2Ru(dpp)\}_2RhCl_2]^{5+}$ trimetallic complex (**Table 1.2**) while the $[(bpy)_2Ru(dpp)RhCl_2(^tBu_2bpy)](PF_6)_3$ bimetallic complex does not photocatalyze water reduction under identical conditions.[7h] The σ-donating properties of the *tert*-butyl

substituent increase electron density at Rh, debilitating electron collection and catalytic activity at the Rh.

Table 1.2: H_2 production with $[\{(Ph_2phen)_2Ru(dpp)\}_2RhCl_2](PF_6)_5$ and $[(Ph_2phen)_2Ru(dpp)RhCl_2(Ph_2phen)](PF_6)_3$ in CH_3CN, with 65 µM photocatalyst, 1.5 M DMA, 0.62 M H_2O and 0.11 mM $[CF_3SO_3^-]$-$[DMAH^+]$ after 20 h photolysis with 470 nm light.

Complex [a]	**TON** [b]	**Volume H_2 (mL)**
$[(Ph_2phen)_2Ru(dpp)RhCl_2(Ph_2phen)](PF_6)_3$	70 ± 10	0.48 ± 0.08
$[\{(Ph_2phen)_2Ru(dpp)\}_2RhCl_2](PF_6)_5$	150 ± 10	1.1 ± 0.1

[a] Ref 7h. [b] mol H_2/mol catalyst.

Ligands on Rh that are stronger σ-donors decrease the Rh characteristic of the LUMO. The reported electrochemical analysis of $[(Ph_2phen)_2Ru(dpp)RhCl_2(^tBu_2bpy)](PF_6)_3$, $[(Ph_2phen)_2Ru(dpp)RhCl_2(Ph_2phen)](PF_6)_3$ and $[(Ph_2phen)_2Ru(dpp)RhBr_2(Ph_2phen)](PF_6)_3$ claims orbital inversion of the LUMO with terminal ligand variation (**Figure 1.13**).[7g] The stronger σ-donating $^tBu_2bpy$ ligand destabilizes the Rh-based e_g* MOs and the first cathodic current observed is a reversible ligand-based reduction. The first reduction potential in both $[(Ph_2phen)_2Ru(dpp)RhCl_2(Ph_2phen)](PF_6)_3$ and $[(Ph_2phen)_2Ru(dpp)RhBr_2(Ph_2phen)](PF_6)_3$ is non-reversible, indicating a follow-up chemical reaction upon reduction (**Figure 1.13**).[7g] The phenyl substituents in the Ph_2phen ligand are electron-withdrawing by induction, decreasing the σ-donating ability of the phenanthroline. The Rh-based e_g* MOs, which are filled during population of the ^{3}MMCT excited state, are lower in energy with the Ph_2phen terminal ligand than the $^tBu_2bpy$ terminal ligand and the Rh(Ph_2phen) complexes are active water reduction catalysts.

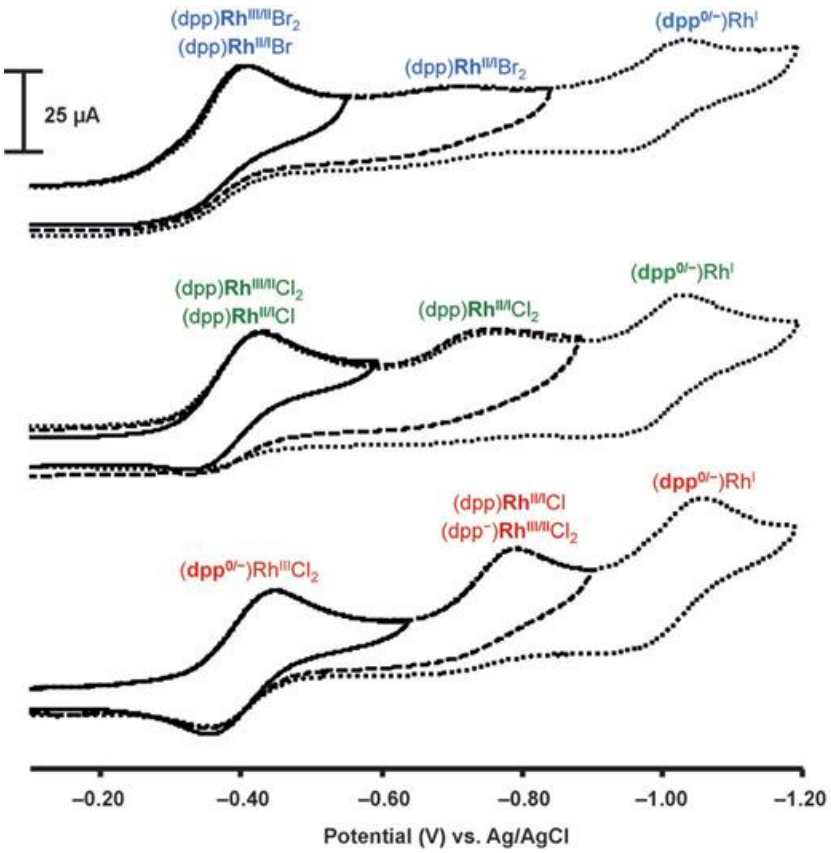

Figure 1.13: Cyclic voltammograms of $[(Ph_2phen)_2Ru(dpp)RhBr_2(Ph_2phen)](PF_6)_3$ (blue), $[(Ph_2phen)_2Ru(dpp)RhCl_2(Ph_2phen)](PF_6)_3$ (green) and $[(Ph_2phen)_2Ru(dpp)RhBr_2(^tBu_2bpy)](PF_6)_3$ (red) with 0.1 M Bu_4NPF_6 in CH_3CN supporting electrolyte. The scan rate applied was 100 $mV \cdot s^{-1}$. This image is copied from reference 7g.

The first cathodic couple for bimetallic complexes with the Ph_2phen ligand on Rh involves $Rh^{III/II}$ reduction which is followed by halide loss. The second reduction potential is assigned as a $Rh^{II/I}X_2$ reduction, where X = Cl or Br.[7g] The existence of the second peak current demonstrates that halide loss upon initial reduction is incomplete in these systems. There are multiple mechanisms following the first reduction of Rh.

The ratio of the second to first peak currents over varying scan rates provides information about the concentration of the fully halogenated species after the first reduction and the rate of halide loss. The Randles-Sevcik equation is limited to fully reversible reductions (**eq. 1.7**), so the information obtained through plots of i_p vs. $v^{1/2}$ for non-reversible reductions is merely qualitative. The $i_p^{c}{}_{(II)}/i_p^{c}{}_{(I)}$ ratio vs. $v^{1/2}$ provides an approximate ratio of the concentration of $Rh^{II}X_2$ to the concentration of unreduced

bimetallic, if all other terms remain constant. However, multiple mechanisms with differing numbers of electrons complicate the equation.

$$i_p = (Constant)nFAC\left(\frac{nFvD}{RT}\right)^{1/2} \quad \textbf{(1.7)}$$

The σ-donating ability of coordinated halide affects catalytic activity. The $i_p{}^c{}_{(II)}/i_p{}^c{}_{(I)}$ ratio increases with increasing σ-donating ability of ligands (**Figure 1.14**).[7g] A smaller value of $i_p{}^c{}_{(II)}$ indicates lower concentration of $Rh^{(II)}X_2$ and a greater percentage of halide loss upon the first reduction. The $[(Ph_2phen)_2Ru(dpp)RhBr_2(Ph_2phen)](PF_6)_3$ bimetallic complex has the weakest σ-donating ligands and the fastest rate of halide loss since a lesser amount of energy is required to populate the e_g^* antibonding MO.

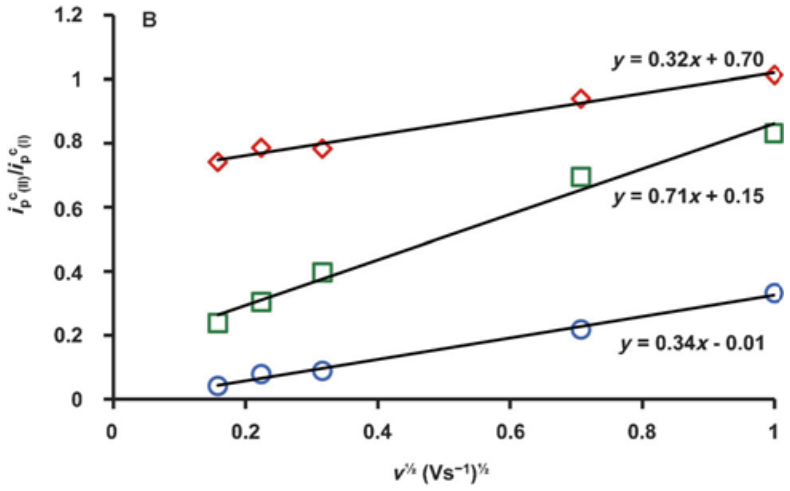

Figure 1.144: Ratio of the second cathodic peak current to the first cathodic peak current vs. the square root of scan rate for $[(Ph_2phen)_2Ru(dpp)RhCl_2(^tBu_2bpy)](PF_6)_3$ (red diamonds), $[(Ph_2phen)_2Ru(dpp)RhCl_2(Ph_2phen)](PF_6)_3$ (green squares) and $[(Ph_2phen_2Ru(dpp)RhBr_2(Ph_2phen)](PF_6)_3$ (blue circles) with 0.1 M Bu_4NPF_6 in CH_3CN supporting electrolyte. This image is copied from reference 7g.

1.7. Thesis Statement

The σ-donating ability of the ligands on Rh has been shown to affect catalytic activity of Ru(II),Rh(III) bimetallic complexes. The electron-withdrawing substituent, carbomethoxy, decreases the pK_a and the σ-donating ability of protonated pyridine (**Table 1.3**).[22] Carbomethoxy will be placed on the 4,4′ position of 2,2′-bipyridine. The

substituted terminal ligand on Rh will stabilize Rh-based e_g* MOs. Lowering the energy of Rh-based e_g* MOs coincides with stabilization of the ^{3}MMCT excited state and increasing k_{et}. Bimetallic complexes with more electron-donating terminal ligands on Rh, 4,4′-dimethyl-2,2′-bipyridine and 2,2′-bipyridine, will be compared with the bimetallic complex with a 4,4′-dicarbomethoxy-2,2′-bipyridine terminal ligand on Rh (**Figure 1.15**). The bimetallic complex with an electron-withdrawing substituent on the terminal ligand will produce more H_2 than the complexes with electron-donating substituents.

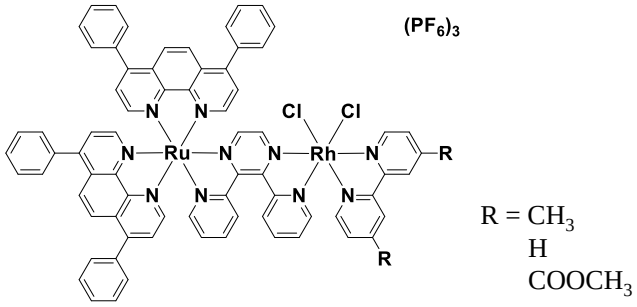

Figure 1.15: Chemical structures of the bimetallic complexes $[(Ph_2phen)_2Ru(dpp)RhCl_2(Me_2bpy)](PF_6)_3$, $[(Ph_2phen)_2Ru(dpp)RhCl_2(bpy)](PF_6)_3$ and $[(Ph_2phen)_2Ru(dpp)RhCl_2(dcmbpy)](PF_6)_3$ (Ph_2phen = 4,7-diphenyl-1,10-phenanthroline; dpp = 2,3-bis(2-pyridyl)pyrazine; Me_2bpy = 4,4′-dimethyl-2,2′-bipyridine; bpy = 2,2′-bipyridine; dcmbpy = 4,4′-dicarbomethoxy-2,2′-bipyridine).

Table 1.3: Listed pK_a values for the conjugate acid of substituted pyridines.

Conjugate Base	**pK_a of Conjugate Acid**	**Reference**
Pyridine	5.17	22 b
4-methylpyridine	6.05	22 a
4-carbomethoxypyridine	3.38	22 a

2. Experimental

2.1. General Methods

Reagent grade solvents, purchased from Spectrum Chemicals, were used without further purification with the exception of spectrophotometric grade acetonitrile used in spectroscopy experiments. Metal chloride salts, Ph_2phen and bpy (Aldrich) and Me_2bpy (Atomax Chemicals) were used as received. Stationary phases for chromatography were commercially obtained. Activated neutral alumina was purchased from Alfa Aesar and

deactivated with methanol. Sephadex® LH-20 resin was purchased from Aldrich and used as received. The 4,4′-dicarbomethoxy-2,2′-bipyridine (dcmbpy) ligand was synthesized similar to the literature for 4,4′-dicarboethoxy-2,2′-bipyridine, substituting methanol for ethanol.[23] $(Ph_2phen)_2RuCl_2$ and $[(Ph_2phen)_2Ru(dpp)](PF_6)_2$ were prepared according to published procedures and the cyclic voltammograms of the products compared with literature values.[24] $(Me_2bpy)RhCl_3 \cdot DMF$ was synthesized similarly to a reported procedure and the product extracted with chloroform.[25] Attempts to synthesize $(bpy)RhCl_3 \cdot DMF$ resulted in low yields. The $[(bpy)RhCl_3 \cdot MeOH](MeOH)$ complex was synthesized according to literature methods.[19,26]

2.2. Synthetic Procedures

2.2.1. Preparation of $(dcmbpy)RhCl_3 \cdot DMF$

The new Rh monometallic complex was synthesized similarly to reported procedure for $(bpy)RhCl_3 \cdot DMF$.[25] $RhCl_3 \cdot xH_2O$ (0.20 g, 0.76 mmol) and 4,4'-dicarbomethoxy-2,2′-bipyridine (0.26 g, 0.92 mmol) were dissolved in 2 mL dimethylformamide and heated in an oil bath at 60 °C for 2h. The solution was cooled to room temperature and added to stirred diethyl ether (200 mL) to induce precipitation. The precipitate was collected on a filter using suction and then dissolved in chloroform and rinsed through the filter into a clean flask. Evaporation of the filtrate yielded 0.34 g, 0.61 mmol, 79% yield of a yellowish-orange solid. ESI-MS: $[M + NH_4]^+$ m/z = 570.98.

2.2.2. Preparation of $[(Ph_2phen)_2Ru(dpp)RhCl_2(Me_2bpy)](PF_6)_3$

The new Ru(II),Rh(III) bimetallic complex was synthesized similarly to previously reported $[(bpy)_2Ru(dpp)RhCl_2(bpy)](PF6)_3$.[27] $[(Ph_2phen)_2Ru(dpp)](PF_6)_2$ (0.48 g, 0.37 mmol) and $(Me_2bpy)RhCl_3 \cdot DMF$ (0.24 g, 0.51 mmol) were dissolved in 30 mL 2:1 ethanol/water (v/v) and heated at reflux for 3 h. After cooling, the solution was precipitated in 200 mL saturated aqueous NH_4PF_6. The precipitate was collected on a filter with suction and washed with 500 mL of water then 100 mL of diethyl ether. The dry, crude product was purified using size exclusion chromatography on Sephadex® LH-20 resin. The sample was loaded as a concentrated acetonitrile and eluted with a 2:1 ethanol/acetonitrile (v/v) solvent mixture. Eight fractions were collected and analyzed with electronic absorption and emission. Fractions 4 - 6 which did not emit at 680 nm

when excited at 520 nm and had matching electronic absorbance spectra were combined. Purified product was dissolved in minimal acetonitrile and precipitated in diethyl ether. Final product was air-dried, yielding 0.10 g, 0.074 mmol, 15% of a dark red solid. ^{1}H NMR analysis was complicated by multiple stereo and geometric isomers. ESI-MS: $[M - PF_6]^+$ m/z = 1647.12. UV-vis (CH_3CN): λ_{max} = 512 nm ($\varepsilon = 2.0 \times 10^4$ $M^{-1}cm^{-1}$).

2.2.3. Preparation of $[(Ph_2phen)_2Ru(dpp)RhCl_2(bpy)](PF_6)_3$

The new Ru(II),Rh(III) bimetallic complex was synthesized similarly to previously reported $[(bpy)_2Ru(dpp)RhCl_2(bpy)](PF6)_3$.[27] $[(Ph_2phen)_2Ru(dpp)](PF_6)_2$ (0.47 g, 0.37 mmol) and $[(bpy)RhCl_3 \cdot MeOH](MeOH)$ (0.21 g, 0.50 mmol) were dissolved in 30 mL 2:1 ethanol/water (v/v) and heated at reflux for 3 h. After cooling, the solution was precipitated in 200 mL saturated aqueous NH_4PF_6. The precipitate was collected on a filter and washed with 500 mL of water then 100 mL of diethyl ether. The dry, crude product was purified using size exclusion chromatography on Sephadex® LH-20 resin. The sample was loaded as a concentrated acetonitrile solution and eluted with a 2:1 ethanol/acetonitrile (v/v) solvent mixture. Nine fractions were collected and analyzed with electronic absorption and emission. Fractions 3 - 5 which did not emit at 680 nm when excited at 520 nm and had matching electronic absorbance spectra were combined. Purified product was dissolved in minimal acetonitrile and precipitated in diethyl ether. Final product was air-dried, yielding 0.23 g, 0.17 mmol 35% of a deep red solid. ^{1}H NMR was complicated by multiple isomers. ESI-MS: $[M - PF_6]^+$ m/z = 1619.10. UV-vis (CH_3CN): λ_{max} = 512 nm ($\varepsilon = 1.9 \times 10^4$ $M^{-1}cm^{-1}$).

2.2.4. Preparation of $[(Ph_2phen)_2Ru(dpp)RhCl_2(dcmbpy)](PF_6)_3$

The new Ru(II),Rh(III) bimetallic complex was synthesized similarly to previously reported $[(bpy)_2Ru(dpp)RhCl_2(bpy)](PF6)_3$.[27] $[(Ph_2phen)_2Ru(dpp)](PF_6)_2$ (0.48 g, 0.37 mmol) and $(dcmbpy)RhCl_3 \cdot DMF$ (0.29g, 0.51 mmol) were dissolved in 30 mL 2:1 ethanol/water (v/v) and heated at reflux for 3 h. After cooling, the solution was precipitated in 200 mL saturated aqueous NH_4PF_6. The precipitate was collected on a filter and washed with 500 mL of water then 100 mL of diethyl ether. The dry, crude product was purified using size exclusion chromatography on Sephadex® LH-20 resin. The sample was loaded as a concentrated acetonitrile solution and eluted with a 2:1

ethanol/acetonitrile (v/v) solvent mixture. Eight fractions were collected and analyzed with electronic absorption and emission. Fractions 3 - 5 which did not emit at 680 nm when excited at 520 nm and had matching electronic absorbance spectra were combined. Purified product was dissolved in minimal acetonitrile and precipitated in diethyl ether. Final product was air-dried, yielding 0.12 g, 0.083 mmol 18% of a deep red solid. ^{1}H NMR was complicated by multiple geometric and stereo isomers. ESI-MS: $[M - PF_6]^+$ m/z = 1735.10. UV-vis (CH_3CN): λ_{max} = 520 nm ($\varepsilon = 1.8 \times 10^4\ M^{-1}cm^{-1}$).

2.3. Experimental Methods

2.3.1. Electrochemistry

Electrochemical experiments were performed in a single cell fitted with a glassy-carbon working electrode, a Pt wire auxiliary and a Ag/AgCl reference electrode calibrated with ferrocene ($E° = 0.46$ V vs. Ag/AgCl). The supporting electrolyte was 0.1 M Bu_4NPF_6 in spectrophotometric grade acetonitrile. The solution was purged with acetonitrile-saturated argon prior to CV scans and blanketed with acetonitrile-saturated argon during scans. Variable scan rate CV was performed with a Princeton Applied Research (PAR) model 283 potentiostat. Electrochemistry was also performed on a Bioanalytical Systems (BAS) Epsilon potentiostat. DigiSim software was used to model CVs obtained with the BAS potentiostat due to insufficient iR compensation. A reversible electrochemical step followed by an irreversible chemical step was entered in DigiSim as **eq. 2.1** and **eq. 2.2**. Both 100 $mV \cdot s^{-1}$ and 1000 $mV \cdot s^{-1}$ were modeled and compared with experimental CVs. The modelled equilibrium constant (K_{eq}) was 1×10^{10}. Internal resistance, the $E_{1/2}$ and the rate constant for the forward chemical reaction were adjusted to match the experimental voltammograms.

$$A + e^- = B \qquad (\mathbf{2.1})$$

$$B = C \qquad (\mathbf{2.2})$$

2.3.2. Electronic Absorption Spectroscopy

The extinction coefficients were determined by measuring the absorption of known concentrations. Each bimetallic complex (20 to 30 mg) was dissolved in 25.00 mL

spectrophotometric grade acetonitrile. The solution was sonicated for a minimum of 30 seconds. Three aliquots (0.750 to 1.000 mL) were diluted to 10.00 mL to obtain a final concentration of about 4.5×10^{-5} M. The electronic absorption of each diluted sample was measured in a Starna 0.2 cm quartz cell using a Hewlett-Packard 8452A diode array spectrophotometer. Each experiment was repeated twice. Extinction coefficients were calculated with **eq. 2.3** in which ε is the extinction coefficient, A is absorption, C is concentration and l is path length of the cell.

$$\varepsilon = \frac{A}{Cl} \tag{2.3}$$

2.3.3. Steady-State Emission Spectroscopy

Emission spectra were collected with a Quanta Master Model QM-200-45E fluorimeter from Photon Technologies, Incorporated. A water-cooled 150 W Xenon arc lamp excitation source was used to excite samples in a 1 cm Starna quartz cell and a thermoelectric-cooled Hamamatsu R2658 photomultiplier tube was employed to detect emission at a 90° angle to the excitation source. Room temperature experiments were performed on molecules of interest dissolved in spectrophotometric grade acetonitrile. The absorption of all samples was about 0.3 a.u. Samples were purged with argon for 10 min in a 1 cm Starna quartz cell fitted with a screw top. The Φ^{em} of Ru(II),Rh(III) bimetallic complexes were determined by referencing the emission of the sample to [Os(bpy)3](PF6)2 ($\Phi^{em} = 4.62 \times 10^{-3}$) (**eq. 2.4**).[28] Emission profiles were corrected for PMT response (**Figure 2.1**).

$$\Phi^{em}_{samp} = (\Phi^{em}_{ref})\left(\frac{Area_{samp}}{Area_{ref}}\right)\left(\frac{Absorbance_{ref}}{Absorbance_{samp}}\right) \tag{2.4}$$

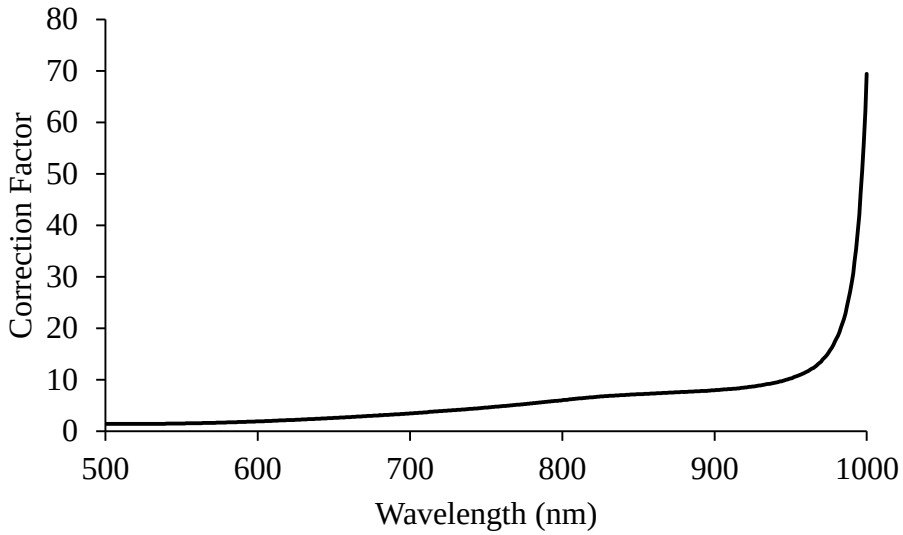

Figure 2.1: Correction factor for PMT response in the 500 to 1000 nm wavelength range.

2.3.4. Time-Resolved Emission Spectroscopy

Time-resolved spectroscopy experiments were completed by Theodore Canterbury at Virginia Tech. The lifetime of the ^{3}MLCT excited state was measured with a tunable dye (PL-201) N_2 laser (PL-2300) from Photon Technologies, Incorporated. Samples with an absorption of about 0.3 were prepared in a Starna 1 cm quartz cell in spectrophotometric grade acetonitrile and purged with argon for 10 min. The lifetimes of the complexes were determined with a mono-exponential decay fit (**eq. 2.5**) of emission intensities vs. time in OriginPro8.

$$y = y_0 + Ae^{-x/\tau} \quad \textbf{(2.5)}$$

2.3.5. Photocatalytic Water Reduction

Photolysis experiments were performed in triplicate inside 20-mL cells fitted with air-tight septa. Catalyst solutions were prepared in spectrophotometric grade DMF and concentrations determined with electronic absorption spectroscopy. Solutions were purged with argon for 10 min prior to addition of the sacrificial electron donor, dimethyl aniline (DMA). The DMA was separately purged with argon for 10 min. The reaction

volumes were 14.5 mL (130 μM catalyst, 0.62 M H_2O, 1.5 M DMA and 0.11 mM [$DMAH^+$]-[$CF_3SO_3^-$]), leaving a 15.5 mL headspace. Solutions were photolyzed with a 470 nm LED light source for 24 hours. Hydrogen production was monitored with HY-OPTIMA 700 H_2 sensors from H_2scan.

3. Results and Discussion

3.1. General Overview

The supramolecular complexes $[(Ph_2phen)_2Ru(dpp)RhCl_2(Me2bpy)](PF_6)_3$, $[(Ph_2phen)_2Ru(dpp)RhCl_2(bpy)](PF_6)_3$ and $[(Ph_2phen)_2Ru(dpp)RhCl_2(dcmbpy)](PF_6)_3$ were synthesized using a building block approach. The three complexes were characterized with ESI mass spectrometry. The large number of geometric and stereoisomers, however, prevented characterization with NMR spectroscopy or x-ray crystallography. The electrochemical and photophysical properties of these complexes were analyzed prior to testing them for photocatalytic water reduction. The results show interesting differences between the carbomethoxy substituted catalyst and the other two complexes.

3.2. Synthesis

The bimetallic complexes discussed herein were synthesized with a building block approach (**Figure 3.1**) to increase purity of the final product. The Ru starting material, $(Ph_2phen)_2RuCl_2$, and the Ru monometallic complex, $[(Ph_2phen)_2Ru(dpp)](PF_6)_2$ were purified with alumina chromatography to remove $[Ru(Ph_2phen)_3](PF_6)_2$ and $[\{(Ph_2phen)_2Ru\}_2(dpp)](PF_6)_4$, respectively. The Rh monometallic complex was purified by solubility differences from the starting materials and byproduct. The desired Rh monometallic complex is soluble in $CHCl_3$ while the $RhCl_3$ starting material and Rh-Rh dimer byproduct do not dissolve in $CHCl_3$. The bimetallic complexes were purified with size exclusion chromatography to remove any residual monometallic reagent. Identity of the product was confirmed with ESI mass spectrometry (**Appendix**) and purity ascertained with emission spectroscopy. The $[Ru(Ph_2phen)_3]^{2+}$ monometallic reagent emits with λ_{max} = 680 nm while the bimetallic complexes emit near 800 nm. Although size exclusion chromatography resulted in high purity, significant product mass was lost and synthetic yields were low.

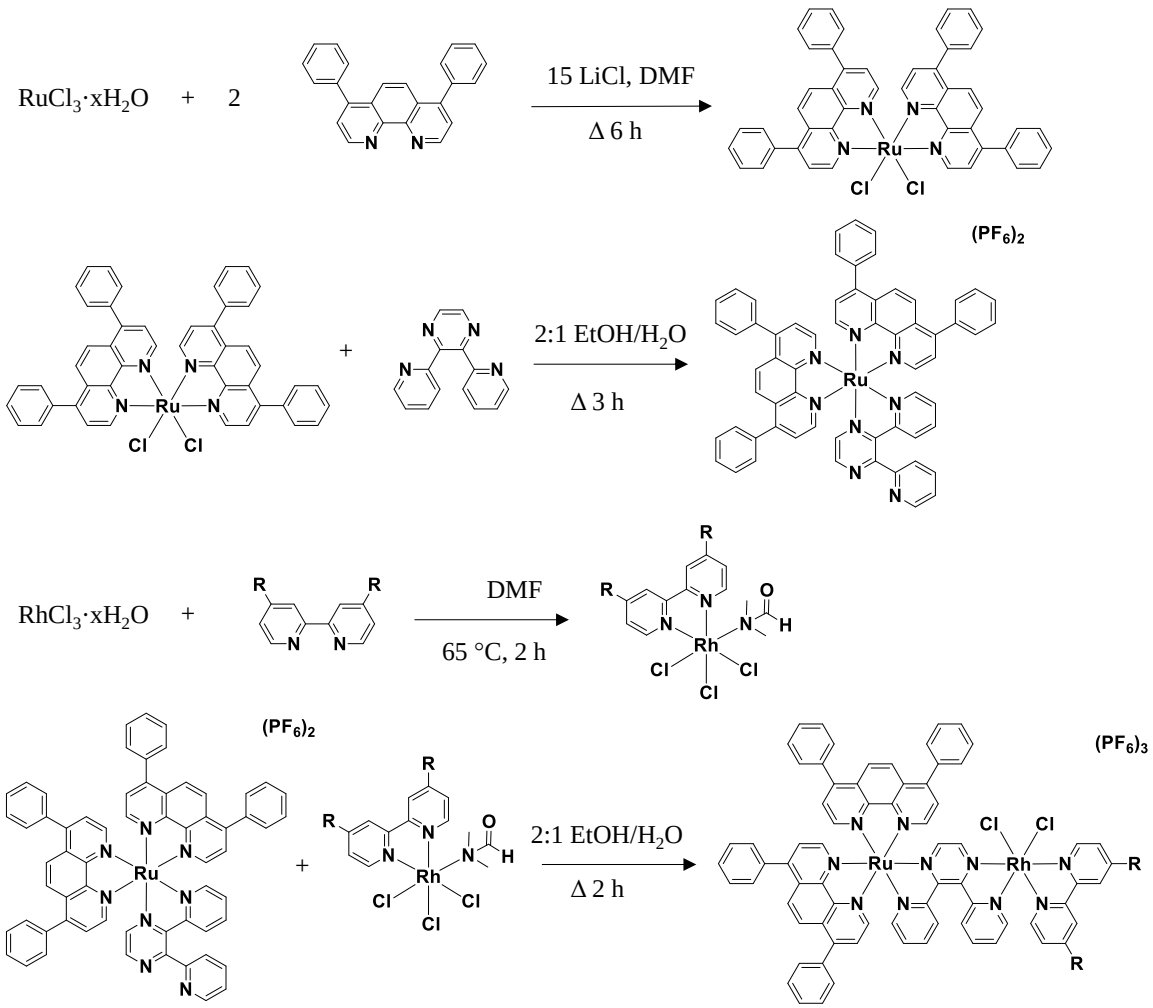

Figure 3.1: Synthetic scheme for $[(Ph_2phen)_2Ru(dpp)RhCl_2(R_2bpy)](PF_6)_3$ (Ph_2phen = 4,7-diphenyl-1,10-phenanthroline; dpp = 2,3-bis(2-pyridyl)pyrazine; R_2bpy = 4,4′-disubstituted-2,2′-bipyridine where the substituent is CH_3, H or $COOCH_3$.

3.3. Electrochemistry

Electrochemical data indicates significant differences in the reductive mechanisms of the three complexes in the series (**Table 3.1** and **Figure 3.2**). The $Ru^{III/II}$ oxidation potential remains constant within the series, indicating that the energy of the Ru-based HOMO is not affected by terminal ligand at Rh. The cathodic region suggests complex kinetics with two possible mechanistic pathways following the $Rh^{III/II}Cl_2$ reduction for all three complexes. The first reduction is reversible when an electrochemical step is followed by a second electrochemical step prior to a chemical reaction (EEC). A non-reversible reduction occurs with an electrochemical step followed by an irreversible chemical process prior to a second electrochemical step (ECE).

Table 3.1: Electrochemical potentials of $[(Ph_2phen)_2Ru(dpp)RhCl_2(Me_2bpy)](PF_6)_3$, $[(Ph_2phen)_2Ru(dpp)RhCl_2(bpy)](PF_6)_3$ and $[(Ph_2phen)_2Ru(dpp)RhCl_2(dcmbpy)](PF_6)_3$.

Complex	E_p^*	E_p^*	$E_{1/2}^*$	**Assignment**
$[(Ph_2phen)_2Ru(dpp)RhCl_2(Me_2bpy)](PF_6)_3$	1.59	1.52	1.56	$Ru^{III/II}$
	−0.37	−0.44	−0.41	$Rh^{III/II}Cl_2$
		−0.82		$Rh^{II/I}Cl_2$
	−0.96	−1.08	−1.02	$(dpp^{0/-})Rh^{I}$
$[(Ph_2phen)_2Ru(dpp)RhCl_2(bpy)](PF_6)_3$	1.60	1.49	1.55	$Ru^{III/II}$
	−0.38	−0.44	−0.41	$Rh^{III/II}Cl_2$
		−0.80		$Rh^{II/I}Cl_2$
	−0.91	−1.11	−1.01	$(dpp^{0/-})Rh^{I}$
$[(Ph_2phen)_2Ru(dpp)RhCl_2(dcmbpy)](PF_6)_3$	1.61	1.48	1.55	$Ru^{III/II}$
		−0.41		$Rh^{III/II}Cl_2$
				$Rh^{II/I}Cl$
		−0.68		$Rh^{II/I}Cl_2$
	−0.92	−1.13	−1.03	$dpp^{0/-}$

* CVs performed with a glassy carbon working electrode, Pt wire auxiliary, and Ag/AgCl reference in 0.1 M Bu_4NPF_6 supporting electrolyte. Potentials reported as V vs. Ag/AgCl.

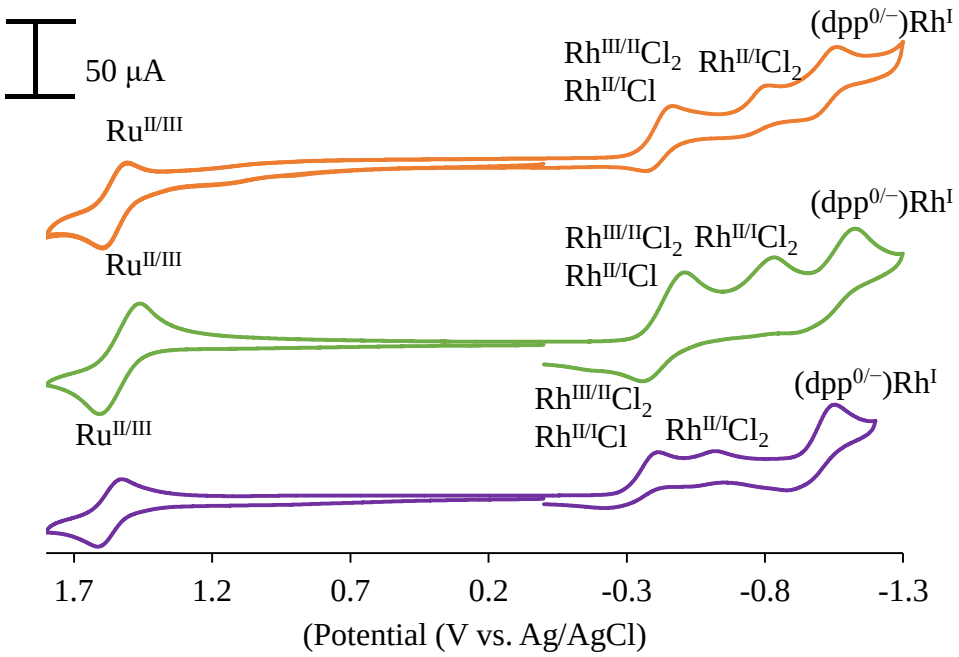

Figure 3.2: Cyclic voltammograms of $[(Ph_2phen)_2Ru(dpp)RhCl_2(Me_2bpy)](PF_6)_3$ (orange), $[(Ph_2phen)_2Ru(dpp)RhCl_2(bpy)](PF_6)_3$ (green) and $[(Ph_2phen)_2Ru(dpp)RhCl_2(dcmbpy)](PF_6)_3$ (purple) with 0.1 M Bu_4NPF_6/CH_3CN supporting electrolyte and a 100 mV/s applied scan rate.

The electron-withdrawing ability of the terminal ligand on Rh dictates which of the two mechanisms is dominant, although both mechanisms occur to some extent in all three molecules. An EEC mechanism is dominant in the $[(Ph_2phen)_2Ru(dpp)RhCl_2(Me_2bpy)](PF_6)_3$ and $[(Ph_2phen)_2Ru(dpp)RhCl_2(bpy)](PF_6)_3$ complexes while the predominant mechanism at slow scan rates in $[(Ph_2phen)_2Ru(dpp)RhCl_2(dcmbpy)](PF_6)_3$ is ECE . In the EEC mechanism, the $Rh^{II}Cl_2$ species is stabilized by the electron-donating terminal ligands on Rh and a separate $Rh^{II/I}Cl_2$ reduction is observed at −0.8 V vs. Ag/AgCl. Rapid halide loss occurs upon $Rh^{III/II}Cl_2$ reduction in the ECE mechanism. The $Rh^{II/I}Cl$ reduction following initial halide loss overlaps with the $Rh^{III/II}Cl_2$ reduction in the ECE mechanism.

The ECE reductive mechanism is typical in Rh polypyridyl dihalide complexes. The rate of chloride loss in both $[Rh(bpy)_2Cl_2]^+$ and $[Rh(phen)_2Cl_2]^+$ is too fast to be analyzed in the cyclic voltammetry time scale.[21] Even at scan rates as fast as 80 V/s, the $Rh^{III/II/I}$ reduction is irreversible.[21] Electron-donating substitution of the polypyridyl ligand does

not alter the reductive mechanism and $Rh(Me_2bpy)_2Cl_2]^+$ also undergoes a two-electron irreversible reduction.[28b]

Coordination to Ru does not preclude the ECE reductive mechanism in Rh polypyridyl dihalide complexes. As expected, trimetallic Ru_2RhCl_2 polypyridyl complexes lacking electronic communication between the different metals behave electrochemically like comparable monometallic complexes.[29] The reductive mechanism is also ECE in trimetallic Ru_2RhCl_2 polypyridyl complexes in which electronic communication does occur between Ru and Rh.[7a-c]

The ECE reductive mechanism of Rh polypyridyl dihalide complexes is not surprising. Rh^{II} polypyridyl complexes are unstable and rapidly decompose into Rh^{I} and Rh^{III} (**eq. 3.1-3.3**).[30] Rh^{II} is stable in Rh paddlewheel complexes containing polypyridyl ligands and can photocatalyze water reduction.[31] However, Rh^{II} is not observed in the electrochemistry of most polypyridyl Ru(II),Rh(III) bimetallic compounds.[32]

$$[Rh^{III}(bpy)_3]^{3+} + e^- \rightleftharpoons [Rh^{II}(bpy)_3]^{2+} \quad \textbf{(3.1)}$$

$$[Rh^{II}(bpy)_3]^{2+} \rightleftharpoons [Rh^{II}(bpy)_2]^{2+} + bpy \quad \textbf{(3.2)}$$

$$2[Rh^{II}(bpy)_2]^{2+} + 2X^- \rightleftharpoons [Rh^{I}(bpy)_2]^{+} + [Rh^{III}(bpy)_2X_2]^{+} \quad \textbf{(3.3)}$$

Ru(II),Rh(III) bimetallic complexes reported by Brewer are unique in that a separate $Rh^{II/I}X_2$ reduction is observed electrochemically.[7d,7g,7h,27] The presence of the $Rh^{II/I}X_2$ reduction indicates an EEC mechanism in which the rate of halide loss is not as fast on the CV timescale. The first reduction is mixed dpp-Rh in character and overlaps with the $Rh^{II/I}X$ reduction following the initial halide loss. The dominance of dpp or Rh in the first reduction and the tendency to follow an EEC or ECE mechanism are dictated by the electronic properties of the terminal ligands on Rh.[7g,7h] The second reduction is a $Rh^{II/I}X_2$ reduction prior to halide loss.[7g]

The reversibility of the first reductive couple was studied with variable scan rate cyclic voltammetry in order to determine the relative rates of chloride loss within the

series. A correlation between faster rates of halide loss, σ-donating ability of the ligands on Rh and greater photocatalytic activity for water reduction exists among $[(Ph_2phen)_2Ru(dpp)RhCl_2(^tBu_2bpy)](PF_6)_3$ and $[(Ph_2phen)_2Ru(dpp)RhX_2(Ph_2phen)](PF_6)_3$ (X = Cl or Br).[7g,33] Faster chloride loss coincides with less reversible reduction because the chemical step following electrochemical reduction occurs faster than the reverse electrochemical process at slow scan rates.

The rate of chloride loss sometimes occurs on a timescale that can be monitored with cyclic voltammetry.[7g] The ratio of the anodic peak current to the cathodic peak current (i_p^a/i_p^c) has a value of 1.0 for reversible processes. Non-reversible reductions, which are followed by a chemical step, have an i_p^a/i_p^c value less than 1.0. An i_p^a/i_p^c value that increases with increasing scan rate indicates that the follow-up chemical step occurs on a timescale that can be monitored with cyclic voltammetry (**eq. 3.4 and 3.5**).

$$Rh^{III}Cl_2 \underset{e^-}{\overset{e^-}{\rightleftharpoons}} Rh^{II}Cl_2 \qquad (\mathbf{3.4})$$

$$Rh^{II}Cl_2 \underset{}{\overset{k_{-Cl}}{\rightleftharpoons}} Rh^{II}Cl \qquad (\mathbf{3.5})$$

The i_p^a/i_p^c for the first reduction in $[(Ph_2phen)_2Ru(dpp)RhCl_2(Me_2bpy)](PF_6)_3$ and $[(Ph_2phen)_2Ru(dpp)RhCl_2(bpy)](PF_6)_3$ is unity even at slow scan rates, whereas in $[(Ph_2phen)_2Ru(dpp)RhCl_2(dcmbpy)](PF_6)_3$, the ratio is less than 1.0 at slow scan rates and increases with increasing scan rate (**Figure 3.3**). The molecular species in the complexes with methyl-substituted and unsubstituted bipyridine remain mostly intact following the first reduction while the complex with carbomethoxy-substituted bipyridine undergoes a chemical change. The most probable chemical reaction is chloride loss due to a decrease in bonding order. The increasing reversibility of the first reduction with increasing scan rate suggests chloride loss in $[(Ph_2phen)_2Ru(dpp)RhCl_2(dcmbpy)](PF_6)_3$ occurs on the CV timescale.

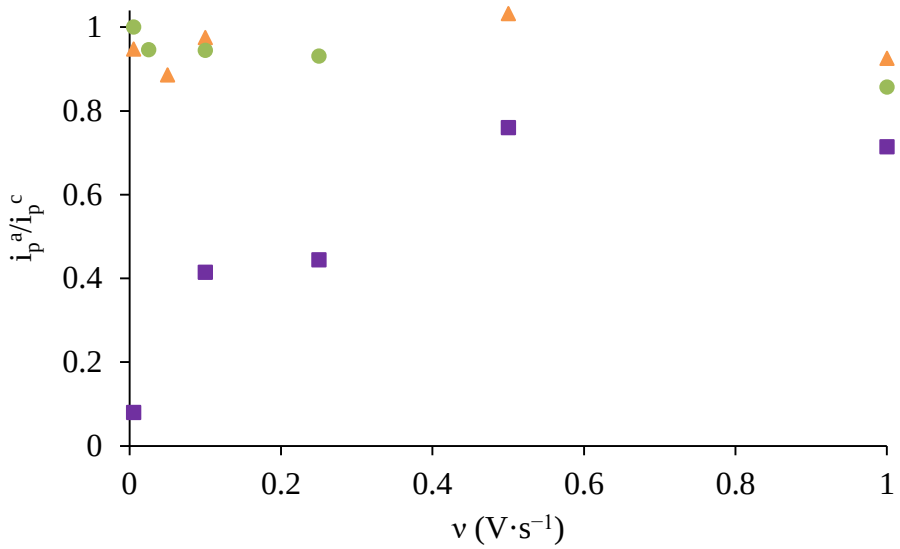

Figure 3.3: Ratio of anodic to cathodic peak current vs. scan rate. Variable scan rate cyclic voltammograms of $[(Ph_2phen)_2Ru(dpp)RhCl_2(Me_2bpy)](PF_6)_3$ (orange triangles), $[(Ph_2phen)_2Ru(dpp)RhCl_2(bpy)](PF_6)_3$ (green circles) and $[(Ph_2phen)_2Ru(dpp)RhCl_2(dcmbpy)](PF_6)_3$ (purple squares) with a glassy carbon working electrode, Pt wire auxiliary, and Ag/AgCl reference in 0.1 M Bu_4NPF_6/CH_3CN supporting electrolyte. Potential sweeps were applied with a BAS potentiostat.

The rate constants for chloride loss following the $Rh^{III/II}$ reduction were quantified with DigiSim modeling for $[(Ph_2phen)_2Ru(dpp)RhCl_2(Me_2bpy)](PF_6)_3$ and $[(Ph_2phen)_2Ru(dpp)RhCl_2(dcmbpy)](PF_6)_3$, the complexes with electron-donating and electron-withdrawing substituents. The DigiSim models overlaid with experimental CVs for $[(Ph_2phen)_2Ru(dpp)RhCl_2(Me_2bpy)](PF_6)_3$ and $[(Ph_2phen)_2Ru(dpp)RhCl_2(dcmbpy)](PF_6)_3$ are shown in **Figure 3.4**. The rate constant for chloride loss in $[(Ph_2phen)_2Ru(dpp)RhCl_2(dcmbpy)](PF_6)_3$ was calculated to be 0.7 s^{-1}. Modeling with rate constants in the 0.6 s^{-1} to 0.8 s^{-1} range and varying internal resistance all produce comparable matches. The return wave in the quasi-reversible reduction does not match perfectly with the model because non-Faradaic current was present in the experimental CV and a blank was not subtracted. The chloride loss rate constant in $[(Ph_2phen)_2Ru(dpp)RhCl_2(Me_2bpy)](PF_6)_3$ is 0.2 s^{-1}. The experimental CV for both complexes shows the onset of a second reduction at −0.6 V vs. Ag/AgCl, precluding a perfect simulation.

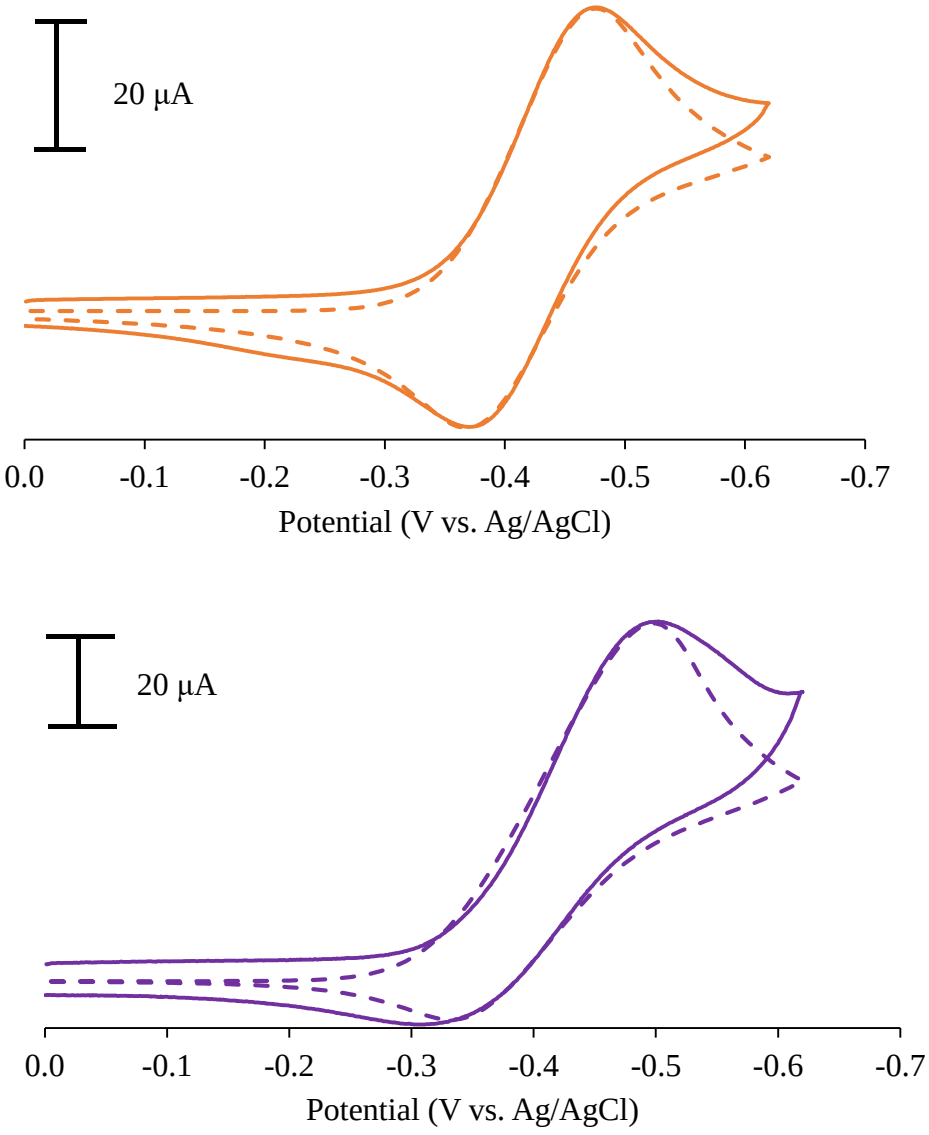

Figure 3.4: DigiSim models (dashed lines) overlaid with experimental CVs (solid lines) for $[(Ph_2phen)_2Ru(dpp)RhCl_2(Me_2bpy)](PF_6)_3$ (orange) and $[(Ph_2phen)_2Ru(dpp)RhCl_2(dcmbpy)](PF_6)_3$ (purple). Experimental CVs were obtained with a 0.1 M Bu_4NPF_6/CH_3CN supporting electrolyte. A potential sweep of 100 mV/s was applied with a BAS potentiostat.

Non-integer peak current ratios for the first and second cathodic couples indicate complicated kinetic mechanisms. Cyclic voltammograms obtained with several scan rates are shown in **Figure 3.5**. The ratio of the second to first cathodic peak ($i_p^{c}{}_{(II)}/i_p^{c}{}_{(I)}$) increases with increasing scan rate (**Figure 3.6**). At faster scan rates, the electrochemical

reaction observed in the second peak is faster than the chemical reaction initiated by the first reduction.

Variation in the slope of the plot of $i_p^c{}_{(II)}/i_p^c{}_{(I)}$ vs. scan rate indicates competitive mechanistic pathways for all three complexes. There are two linear regions in which each mechanism dominates (**Figure 3.6**). The dominant mechanism at slower scan rates is an ECE mechanism with chloride loss following the first reduction. At faster scan rates, the second Rh reduction occurs faster than chloride loss and an EEC mechanism dominates.

The intersection of the two linear regions provides an approximate rate constant for chloride loss. The intersection point for $[(Ph_2phen)_2Ru(dpp)RhCl_2(dcmbpy)](PF_6)_3$ occurs at approximately 0.7 $V \cdot s^{-1}$, consistent with DigiSim modeling. The intersection for $[(Ph_2phen)_2Ru(dpp)RhCl_2(bpy)](PF_6)_3$ is observed at approximately 0.5 $V \cdot s^{-1}$. Two linear regions cannot be distinguished for $[(Ph_2phen)_2Ru(dpp)RhCl_2(Me_2bpy)](PF_6)_3$. Error due to baseline measurements and instrument noise at slow scan rates obscure the intersection point. Nevertheless, a trend of increasing rate of chloride loss with decreasing σ-donating ability of the polypyridyl terminal ligand is observed. More facile population of the antibonding orbital with less σ-donating ligands enables more rapid cleavage of the Rh-Cl bond.

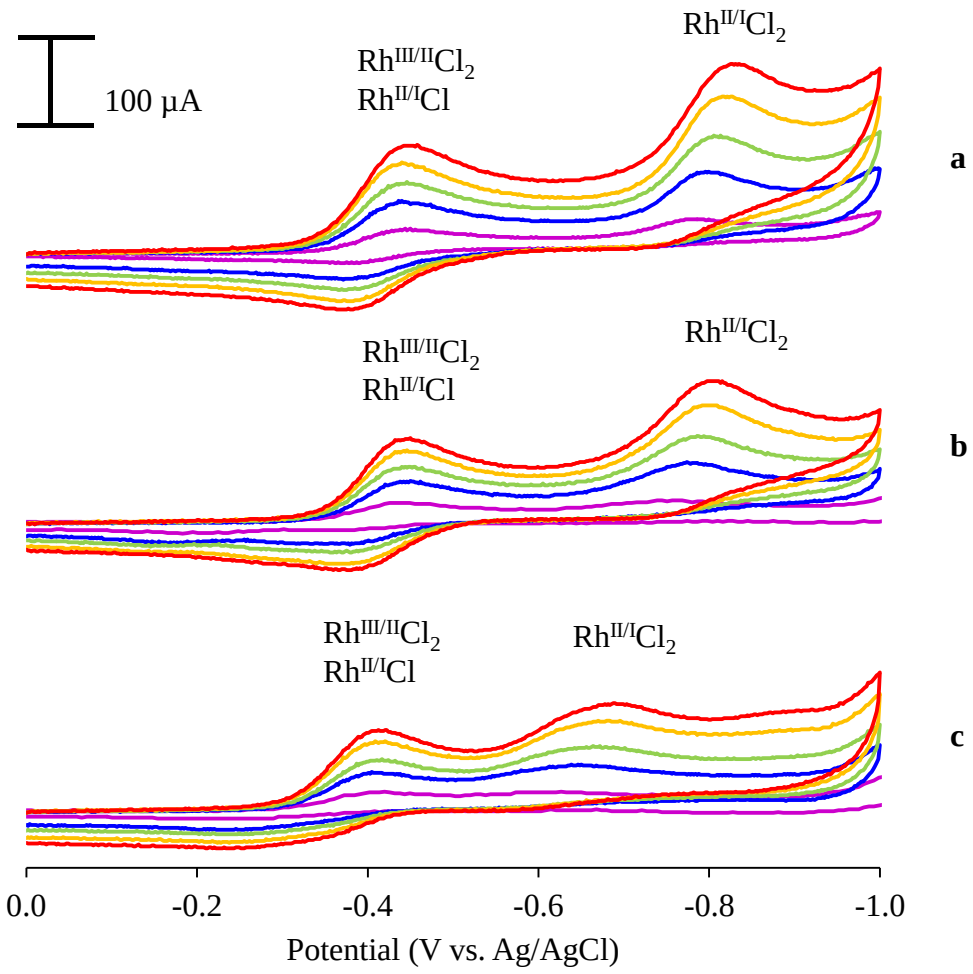

Figure 3.5: Variable scan rate cyclic voltammograms of $[(Ph_2phen)_2Ru(dpp)RhCl_2(Me_2bpy)](PF_6)_3$ (**a**), $[(Ph_2phen)_2Ru(dpp)RhCl_2(bpy)](PF_6)_3$ (**b**) and $[(Ph_2phen)_2Ru(dpp)RhCl_2(dcmbpy)](PF_6)_3$ (**c**) with a glassy carbon working electrode, Pt wire auxiliary, and Ag/AgCl reference in 0.1 M Bu_4NPF_6/CH_3CN supporting electrolyte. A PAR potentiostat with iR compensation was used. CVs shown had an applied scan rate of 100 (purple), 500 (blue), 900 (green), 1500 (orange) and 2000 (red) $mV \cdot s^{-1}$.

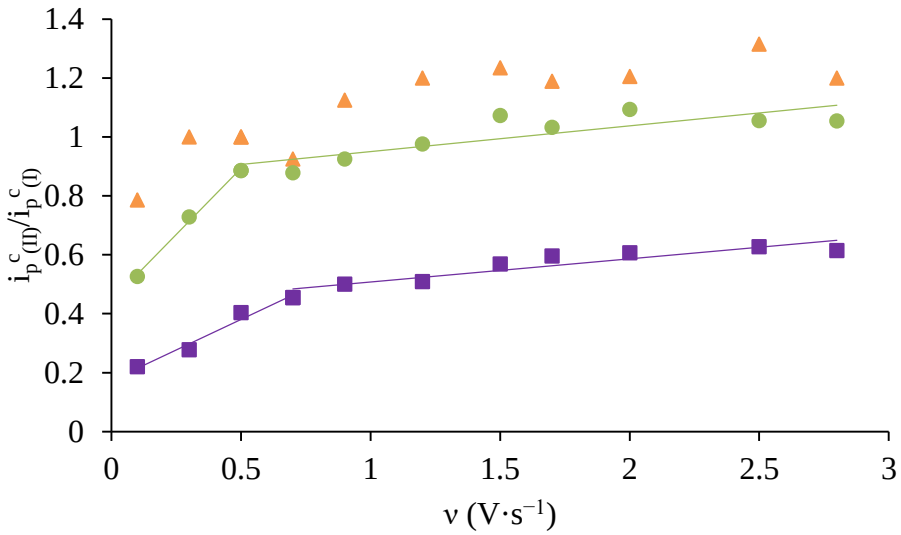

Figure 3.6: Peak current ratio $i_p^{c}{}_{(II)}/i_p^{c}{}_{(I)}$ vs. scan rate for $[(Ph_2phen)_2Ru(dpp)RhCl_2(Me_2bpy)](PF_6)_3$ (orange triangles), $[(Ph_2phen)_2Ru(dpp)RhCl_2(bpy)](PF_6)_3$ (green circles) and $[(Ph_2phen)_2Ru(dpp)RhCl_2(dcmbpy)](PF_6)_3$ (purple squares). A PAR potentiostat with iR compensation was used to apply 100, 300, 500, 700, 900, 1200, 1500, 1700, 2000, 2500 and 2800 mV·s^{-1} scan rates.

The $E_{1/2}$ of the second reduction of $[(Ph_2phen)_2Ru(dpp)RhCl_2(dcmbpy)](PF_6)_3$ is shifted positive compared with the second reduction of $[(Ph_2phen)_2Ru(dpp)RhCl_2(Me_2bpy)](PF_6)_3$ and $[(Ph_2phen)_2Ru(dpp)RhCl_2(bpy)](PF_6)_3$ (**Figure 3.5**). The positive shift by 0.12 V indicates that either the Rh^{II} MOs are stabilized with the electron-withdrawing substituent or the rate of chloride loss following $Rh^{III/II}$ reduction increases.[34] Halide loss is thought to be an important step in the catalytic mechanism of these complexes and a positive shift in the $E_{1/2}$ of the second reduction may correlate with increased hydrogen production.

Variable electron-withdrawing ability of ligands on Rh has been shown to shift the Rh $E_{1/2}$ in several polypyridyl Rh monometallic complexes. Increased electron-withdrawing ability of the halide in $[Rh(bpy)_2X_2]^+$ monometallic complexes results in a positive shift of the $Rh^{III/II/I}$ $E_{1/2}$.[13] Similarly, a positive shift is observed when increasing the aromaticity of polypyridyl ligands.[11]

Substituted bipyridine has been shown to shift the Rh $E_{1/2}$ in mixed-ligand Rh monometallic complexes. Steckhan *et al.* reported positive shifts in Rh $E_{1/2}$ in Rh

polypyridyl pentamethylcyclopentadiene complexes with electron-withdrawing substitution of the bipyridine.[35] A more thorough investigation of ligand electronic effects in [RhCl(Me_5Cp)(X_2bpy)]Cl (Me_5Cp is pentamethylcyclopentadiene; X_2bpy is 4,4′-di-substituted-2,2′-bipyridine) by Lütz *et al*. with eight different substituents in the 4,4′ position demonstrates a strong correlation between electron-withdrawing ability of the substituent on bipyridine and the $E_{1/2}$ of the Rh reduction.[36]

The electron-withdrawing ability of terminal ligands also impacts photochemical reduction of Rh. Sutin and Creutz analyzed the rate constant for emission quenching of $[Ru(bpy)_3]^{2+}$ and $[Ru(phen)_3]^{2+}$ by bipyridinium derivatives and observed an increase in the quenching rate constant as the bipyridinium derivative reduction potential shifts to more positive potentials.[37] Although quenching rate constants were not determined with substituted Rh polypyridyl complexes, reduction potentials of $[Rh(R_2bpy)]^+$ (R_2bpy = 4,4′-di-substituted-2,2′-bipyridine) shifted positive with increased electron-withdrawing ability of the substituent.[37] Since the quenching rate constant increases with a more easily reduced bipyridinium derivative, it may also increase with a more easily reduced $[Rh(R_2bpy)]^+$.

3.4.Electronic Absorption Spectroscopy

The electronic absorption properties of the Ru(II),Rh(III) bimetallic complexes reported herein are consistent with those of previously published Ru(II),Rh(III) bimetallic complexes with a $[(Ph_2phen)_2Ru(dpp)]^{2+}$ light absorbing unit. The UV region is dominated by intraligand transitions ($\pi \rightarrow \pi^*$) (**Figure 3.7**, **Table 3.2**). The highest energy charge transfer excitation is a ^{1}MLCT transition (Ru d$\pi \rightarrow Ph_2$phen π^*) with λ_{max} = 426 nm for all three complexes. The lowest energy excitation is a ^{1}MLCT transition (Ru d$\pi \rightarrow$ dpp π^*) in the visible region with λ_{max} = 512 nm for $[(Ph_2phen)_2Ru(dpp)RhCl_2(Me_2bpy)](PF_6)_3$ and $[(Ph_2phen)_2Ru(dpp)RhCl_2(bpy)](PF_6)_3$ ($\varepsilon = 2.0 \times 10^{-4}$ $M^{-1}cm^{-1}$ and 1.9×10^{-4} $M^{-1}cm^{-1}$, respectively) and λ_{max} = 520 nm ($\varepsilon = 1.8 \times 10^{-4}$ $M^{-1}cm^{-1}$) for $[(Ph_2phen)_2Ru(dpp)RhCl_2(dcmbpy)](PF_6)_3$. Although there are subtle differences, the electronic absorption properties of all complexes studied are nearly identical.

The light absorbing characteristics of these bimetallic complexes are typical of a Ru polypyridyl light absorber covalently coordinated to Rh.[7g,7h,19,27,32-33,38] The Ru dπ → bridging ligand π* transition is red-shifted in Ru compounds coordinated to Rh compared with a Ru polypyridyl complex with an open coordination site. Kalyanasundaram *et al*. report the Ru dπ → dpp π* transition as having λ_{max} = 468 nm in $[(bpy)_2Ru(dpp)](PF_6)_2$ and shifting to 514 nm upon coordination to Rh in $[(bpy)_2Ru(dpp)Rh(bpy)_2](PF_6)_5$.[38b] Coordination to Rh stabilizes the ^{3}MLCT excited state.

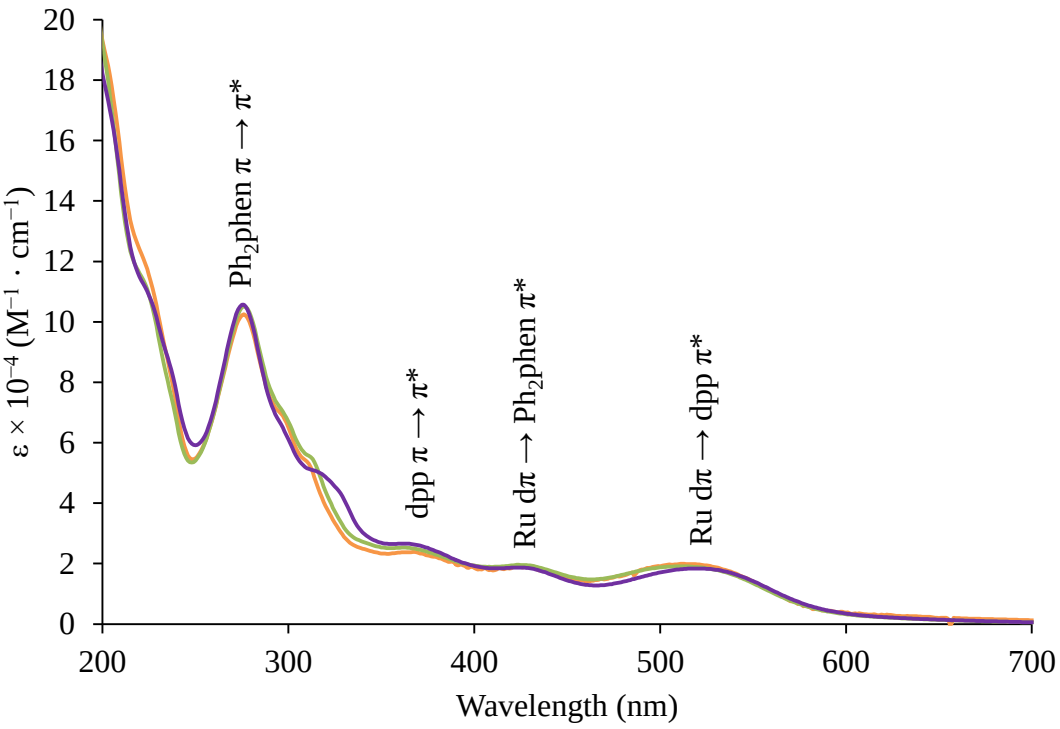

Figure 3.7: Electronic absorption spectra of $[(Ph_2phen)_2Ru(dpp)RhCl_2(Me_2bpy)](PF_6)_3$, $[(Ph_2phen)_2Ru(dpp)RhCl_2(bpy)](PF_6)_3$ and $[(Ph_2phen)_2Ru(dpp)RhCl_2(dcmbpy)](PF_6)_3$ in spectrophotometric grade acetonitrile.

Table 3.2: Electronic absorption properties of $[(Ph_2phen)_2Ru(dpp)RhCl_2(Me_2bpy)](PF_6)_3$, $[(Ph_2phen)_2Ru(dpp)RhCl_2(bpy)](PF_6)_3$ and $[(Ph_2phen)_2Ru(dpp)RhCl_2(dcmbpy)](PF_6)_3$ in spectrophotometric grade acetonitrile at room temperature.

Complex	**λ^{abs} (nm)**	**Assignment**
$[(Ph_2phen)_2Ru(dpp)RhCl_2(Me_2bpy)](PF_6)_3$	273	$Ph_2phen\ \pi \rightarrow \pi^*$
	363	$dpp\ \pi \rightarrow \pi^*$
	426	$Ru\ d\pi \rightarrow Ph_2phen\ \pi^*$
	512	$Ru\ d\pi \rightarrow dpp\ \pi^*$
$[(Ph_2phen)_2Ru(dpp)RhCl_2(bpy)](PF_6)_3$	275	$Ph_2phen\ \pi \rightarrow \pi^*$
	361	$dpp\ \pi \rightarrow \pi^*$
	426	$Ru\ d\pi \rightarrow Ph_2phen\ \pi^*$
	512	$Ru\ d\pi \rightarrow dpp\ \pi^*$
$[(Ph_2phen)_2Ru(dpp)RhCl_2(dcmbpy)](PF_6)_3$	273	$Ph_2phen\ \pi \rightarrow \pi^*$
	368	$dpp\ \pi \rightarrow \pi^*$
	427	$Ru\ d\pi \rightarrow Ph_2phen\ \pi^*$
	520	$Ru\ d\pi \rightarrow dpp\ \pi^*$

3.5. Emission Spectroscopy

The three molecules in the series undergo radiative decay from the ^{3}MLCT excited state as phosphorescence. Excited state emission spectroscopy provides an approximate energy of the ^{3}MLCT excited state. Electronic communication exists between ligands on the same metal in a supramolecular complex.[5] The energy of the ^{3}MLCT excited state may be slightly affected by the energetics of the terminal ligand on Rh. The maximum emission wavelength (λ^{em}) of $[(Ph_2phen)_2Ru(dpp)RhCl_2(dcmbpy)](PF_6)_3$ (787 ± 10 nm) is slightly blue shifted relative to the λ^{em} of $[(Ph_2phen)_2Ru(dpp)RhCl_2(Me_2bpy)](PF_6)_3$ and $[(Ph_2phen)_2Ru(dpp)RhCl_2(bpy)](PF_6)_3$ (808 ± 10 nm) but is nearly within error (**Figure 3.8**, **Table 3.3**). All three complexes have the same light absorbing component ($[(Ph_2phen)_2Ru(dpp)]^{2+}$) so the energy levels of the ^{3}MLCT excited states are expected to be comparable. The slight variance is likely due to electronic communication between dpp and the terminal ligand on Rh.

Quantum yield of emission (Φ^{em}) is the ratio of the number of photon emitted to the number of photons absorbed (**eq. 3.6**). If 100% of the light absorbed populates a given excited state, the Φ^{em} is the ratio of the rate constant for phosphorescence to the sum of all rate constants of deactivation from the excited state (**eq. 3.7**). The ^{3}MLCT excited state of Ru polypyridyl complexes is populated with unit efficiency, based on the studies by Bolletta *et al*. with excited $[Ru(bpy)_3]^{2+*}$ and $S_2O_8^{2-}$, producing SO_4^{2-} with unit efficiency.[39]

$$\Phi^{em} = \frac{\text{photons emitted}}{\text{photons absorbed}} \qquad \textbf{(3.6)}$$

$$\Phi^{em} = \Phi^{pop}\frac{k_p}{k_p + k_{nr} + k_{et}} \qquad \textbf{(3.7)}$$

A greater Φ^{em} is expected for the higher energy ^{3}MLCT excited state of $[(Ph_2phen)_2Ru(dpp)RhCl_2(dcmbpy)](PF_6)_3$ based on the energy gap law, which states that non-radiative decay occurs more slowly when the energy difference between states is greater.[40] The $[(Ph_2phen)_2Ru(dpp)RhCl_2(dcmbpy)](PF_6)_3$ Φ^{em} is $(6.4 \pm 0.6) \times 10^{-4}$, slightly greater than the Φ^{em} of $[(Ph_2phen)_2Ru(dpp)RhCl_2(Me_2bpy)](PF_6)_3$ and $[(Ph_2phen)_2Ru(dpp)RhCl_2(bpy)](PF_6)_3$ ($(5.2 \pm 0.5) \times 10^{-4}$ and $(4.7 \pm 0.5) \times 10^{-4}$, respectively) (**Table 3.3**). Similarly, the quantum yield of $[Ru(dcmbpy)_3]^{2+}$ is greater than that of $[Ru(R_2bpy)_3]^{2+}$ complexes with electron-donating substituents.[41] Although the substituted ligand is coordinated to Rh rather than to Ru, the ester properties appear to affect the Ru to dpp ^{3}MLCT excited state.

A small amount of the emissive Ru monometallic complex, $[(Ph_2phen)_2Ru(dpp)](PF_6)_2$, causes an increase in the Φ^{em} calculation for $[(Ph_2phen)_2Ru(dpp)RhCl_2(Me_2bpy)](PF_6)_3$. In the absence of the $[(Ph_2phen)_2Ru(dpp)](PF_6)_2$ impurity, the emission of $[(Ph_2phen)_2Ru(dpp)RhCl_2(bpy)](PF_6)_3$ and $[(Ph_2phen)_2Ru(dpp)RhCl_2(Me_2bpy)](PF_6)_3$ are probably identical. The quantum yields of the two complexes are within error of one another even with the known impurity.

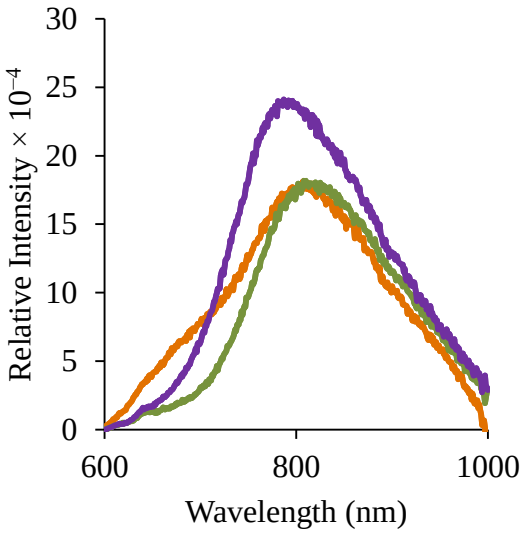

Figure 3.8: Steady-state emission spectra of $[(Ph_2phen)_2Ru(dpp)RhCl_2(Me_2bpy)](PF_6)_3$ (orange), $[(Ph_2phen)_2Ru(dpp)RhCl_2(bpy)](PF_6)_3$ (green), $[(Ph_2phen)_2Ru(dpp)RhCl_2(dcmbpy)](PF_6)_3$ (purple) collected at room temperature in deaerated spectrophotometric grade acetonitrile.

Table 3.3: Summary of room temperature emission spectroscopic data in deaerated acetonitrile.

Complex	**λ^{em} (nm)**	**Φ^{em} ($\times 10^{-4}$)**	**τ (ns)**
$[(Ph_2phen)_2Ru(dpp)RhCl_2(Me_2bpy)](PF_6)_3$	808 ± 10	5.2 ± 0.5	47 ± 5
$[(Ph_2phen)_2Ru(dpp)RhCl_2(bpy)](PF_6)_3$	808 ± 10	4.7 ± 0.5	44 ± 4
$[(Ph_2phen)_2Ru(dpp)RhCl_2(dcmbpy)](PF_6)_3$	787 ± 10	6.4 ± 0.6	93 ± 9

The excited state lifetime (τ) is the time required for the molecule in the ^{3}MLCT excited state to relax back to the ground state. It is the inverse of all forms of deactivation from the ^{3}MLCT excited state. All decay plots fit well ($R^2 > 0.97$) with mono-exponential decay. The τ of $[(Ph_2phen)_2Ru(dpp)RhCl_2(dcmbpy)](PF_6)_3$ is longer-lived (93 ns ± 9 ns) compared with that of $[(Ph_2phen)_2Ru(dpp)RhCl_2(Me_2bpy)](PF_6)_3$ and $[(Ph_2phen)_2Ru(dpp)RhCl_2(bpy)](PF_6)_3$ (47 ns ± 5 ns and 44 ns ± 4 ns, respectively), as shown in **Table 3.3**. Lifetime decay plots are provided in the **Appendix**.

The electron-withdrawing substituent on the terminal ligand on Rh in $[(Ph_2phen)_2Ru(dpp)RhCl_2(dcmbpy)](PF_6)_3$ was expected to stabilize the ^{3}MMCT excited

state and increase the driving force for electron transfer from the ^{3}MLCT excited state. The long lifetime of $[(Ph_2phen)_2Ru(dpp)RhCl_2(dcmbpy)](PF_6)_3$ is unexpected. Assuming the rate constants for radiative and non-radiative decay remain constant with a constant light absorber, the k_{el} in $[(Ph_2phen)_2Ru(dpp)RhCl_2(dcmbpy)](PF_6)_3$ is lesser than in $[(Ph_2phen)_2Ru(dpp)RhCl_2(bpy)](PF_6)_3$ or $[(Ph_2phen)_2Ru(dpp)RhCl_2(Me_2bpy)](PF_6)_3$.

It is possible that the extended lifetime of $[(Ph_2phen)_2Ru(dpp)RhCl_2(dcmbpy)](PF_6)_3$ is due to qualities of the carbomethoxy substituent other than its electron-withdrawing ability. Bipyridyl substitution with both electron-donating and electron-withdrawing groups in $[Ru(R_2bpy)_3]^{2+}$ complexes usually lowers the lifetime and emission quantum yield compared with $[Ru(bpy)_3]^{2+}$ but the lifetime and quantum yield of ruthenium(II) tris-4,4′-biscarboxyethyl-2,2′-bipyridine ($[Ru(deeb)_3]^{2+}$) is significantly greater than other complexes (τ = 1.65 μs for $[Ru(deeb)_3]^{2+}$ compared with τ = 0.25 μs for $[Ru((NO_2)_2bpy)_3]^{2+}$ in 4:1 EtOH/MeOH v/v at room temperature).[42] The ester-substituted complex also has a greater k_r and lower k_{nr} than most $[Ru(R_2bpy)_3]^{2+}$ complexes, accounting for the increased Φ^{em}.[43]

The ^{3}MLCT excited state properties of $[Ru(R_2bpy)_3]^{2+}$ complexes offer some insight into the excited state properties of Ru(II), Rh(III) bimetallic complexes. However, it is important to keep in mind that the ^{3}MLCT excited state properties and deactivation pathways of the complexes studied in this work are significantly different than a Ru substituted polypyridyl monometallic complex. The ^{3}MLCT excited state lifetime of $[(Ph_2phen)_2Ru(dpp)RhCl_2(dcmbpy)](PF_6)_3$ may be extended by decreased non-radiative decay associated with the ester group, which seems doubtful given the distance between the Ru and dcmbpy ligand even though the dpp bridging ligand is influenced. Alternatively, the increased lifetime may be the result of an electron-withdrawing group stabilizing the ^{3}MMCT excited state. Kalyanasundaram *et al.* observed increased excited state lifetimes with increased electron-withdrawing ability of carboxy substituents in $[Ru(R_2bpy)_3]^{2+}$.[44] Although the driving force is increased by stabilization of the ^{3}MMCT excited state, the energy gap increases and k_{et} is a non-radiative process.

3.6. Photocatalytic Water Reduction

All three molecules are active photocatalysts for water reduction (**Figure 3.9**). $[(Ph_2phen)_2Ru(dpp)RhCl_2(dcmbpy)](PF_6)_3$, which has an electron-withdrawing substituent on the Rh terminal ligand, produces significantly more hydrogen than the two complexes without an electron-withdrawing substituent. The turnover number (TON) is reported as moles hydrogen per mole catalyst. After photolysis for 20 hours, the TON with $[(Ph_2phen)_2Ru(dpp)RhCl_2(dcmbpy)](PF_6)_3$ is 63, while it is only 30 with $[(Ph_2phen)_2Ru(dpp)RhCl_2(Me_2bpy)](PF_6)_3$ and 35 with $[(Ph_2phen)_2Ru(dpp)RhCl_2(bpy)](PF_6)_3$. The amount of hydrogen produced with $[(Ph_2phen)_2Ru(dpp)RhCl_2(dcmbpy)](PF_6)_3$ is nearly twice that produced with the complexes that do not have an electron-withdrawing substituent.

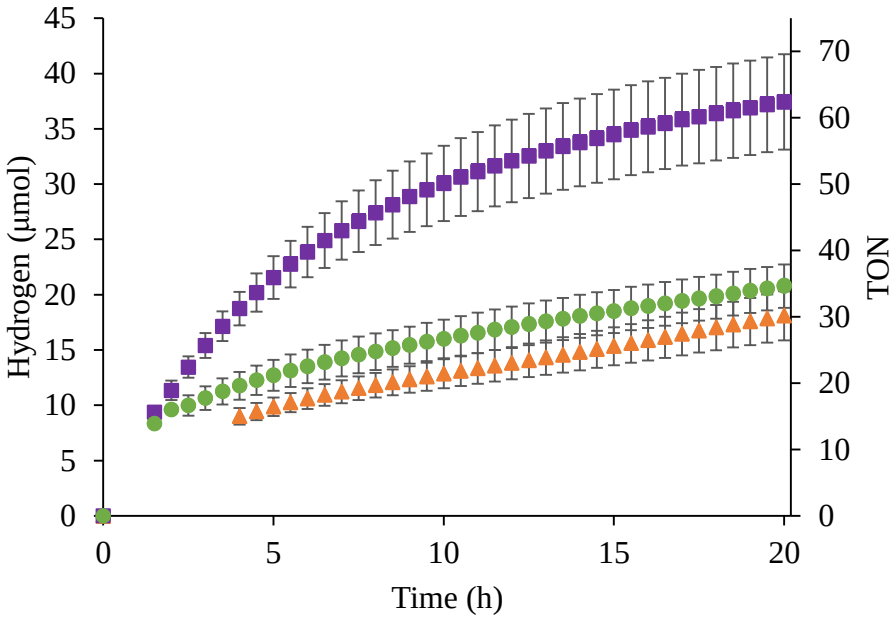

Figure 3.9: Photocatalytically produced hydrogen with $[(Ph_2phen)_2Ru(dpp)RhCl_2(dcmbpy)](PF_6)_3$ (purple squares), $[(Ph_2phen)_2Ru(dpp)RhCl_2(bpy)](PF_6)_3$ (green circles) and $[(Ph_2phen)_2Ru(dpp)RhCl_2(Me_2bpy)](PF_6)_3$ (orange triangles) in DMF. Total solution volume was 4.5 mL (130 μmol catalyst, 0.62 M H_2O, 1.5 M DMA, 0.11 mM $[DMA^+][CF_3SO_3^-]$) and 15.5 mL headspace.

Direct comparison to other photocatalytic systems is difficult and is often misleading. Catalysts that do not involve light absorption can more easily be compared with their

turnover frequencies (TOF), moles product per mole catalyst per unit time. The efficiency of photocatalysis, however, is affected not only by catalyst concentration but also by the concentration of light absorber and the permittivity of light through solution. The ratio of light absorber to catalyst in different systems is rarely the same.

There are indeed numerous reports of photocatalysts for water reduction that are more efficient than the currently examined complexes – both in different and similar systems. Ishitani *et al*. recently reported photocatalytic water reduction with a TOF of 190 h^{-1} based on the amount of light absorber used.[45] The 586 h^{-1} TOF with respect to 5 μM cobalt catalyst concentration reported by Thummel *et al*. decreased to 172 h^{-1} with 20 μM catalyst but a TOF calculation with respect to the 0.4 mM $[Ru(bpy)_3]^{2+}$ light absorber would be even more drastically decreased.[46] Numerous variations in experimental conditions and analysis of results obscure determination of a superior photocatalyst.

Comparison of photocatalysts is most accurately done among similar systems, although slight variations in experimental conditions can convolute collation. The trimetallic complex $[\{(Ph_2phen)_2Ru(dpp)\}_2RhCl_2]^{5+}$ photocatalyzes water reduction with a 7.5 h^{-1} TOF with respect to Rh using 65 μM catalyst.[7c] Photocatalysis with 65 μM $[(Ph_2phen)_2Ru(dpp)RhCl_2(Ph_2phen)](PF_6)_3$ reduces water with a TOF of 3.5 h^{-1} and 130 μM catalyst reduces water with a TOF of 2.5 h^{-1} with respect to Rh.[7h] Subsequent photocatalysis experiments with Ru(II), Rh(III) bimetallic polypyridyl supramolecules have used 130 μM catalyst in order to maintain a consistent number of Ru light absorbing units with previously reported Ru(II), Rh(III), Ru(II) trimetallic photocatalysts.[33]

The $[(Ph_2phen)_2Ru(dpp)RhCl_2(dcmbpy)](PF_6)_3$ complex is not the most efficient photocatalyst (TOF = 3.1 h^{-1} with respect to 130 μM Rh) but valuable information can be gleaned from the photochemical analysis. It has been seen that incorporation of a less σ-donating halide on Rh improves photocatalysis.[7b,7c,33] This work demonstrates enhancement of photocatalytic water reduction with electron-withdrawing substitution of the terminal ligand on Rh. $[(Ph_2phen)_2Ru(dpp)RhCl_2(dcmbpy)](PF_6)_3$ produces a comparable amount of hydrogen as the recently reported $[(Ph_2phen)_2Ru(dpp)RhBr_2(Ph_2phen)](PF_6)_3$ (TOF = 3.1 h^{-1}) under identical experimental conditions.[33]

The electronegativities of the coordinated bromide and the carbomethoxy substituent effectively draw electron density toward the catalytic Rh site. Density functional theory (DFT) calculations of $[Ru(bpy)_2LL]^{2+}$ in which LL is a substituted bipyridine suggest that the LUMO resides primarily on LL with electron-withdrawing substitution.[41] The molecular orbitals in complexes with extensive aromaticity, like $[(Ph_2phen)_2Ru(dpp)RhCl_2(dcmbpy)](PF_6)_3$, are highly delocalized. The LUMO is likely a mixed molecular orbital residing on both the bridging ligand and the Rh metal.[7g] Cyclic voltammetry shows that the LUMO of $[(Ph_2phen)_2Ru(dpp)RhCl_2(Ph_2phen)](PF_6)_3$ is more dpp-based and less Rh-based than the LUMO of $[(Ph_2phen)_2Ru(dpp)RhBr_2(Ph_2phen)](PF_6)_3$ and it is an inferior photocatalyst.[7g,33] The $[(Ph_2phen)_2Ru(dpp)RhCl_2(bpy)](PF_6)_3$ and $[(Ph_2phen)_2Ru(dpp)RhCl_2(Me_2bpy)](PF_6)_3$ complexes which have more reversible LUMO reductions than $[(Ph_2phen)_2Ru(dpp)RhCl_2(dcmbpy)](PF_6)_3$ also catalyze water reduction less efficiently. The electron-withdrawing substituent in the dcmbpy ligand causes the LUMO to be more Rh-based and facilitates water reduction.

The long-lived ^{3}MLCT excited state of $[(Ph_2phen)_2Ru(dpp)RhCl_2(dcmbpy)](PF_6)_3$ also contributes to the enhanced hydrogen production compared with the $[(Ph_2phen)_2Ru(dpp)RhCl_2(Me_2bpy)](PF_6)_3$ and $[(Ph_2phen)_2Ru(dpp)RhCl_2(bpy)](PF_6)_3$ complexes. Photocatalytic water reduction by other polypyridyl Ru(II), Rh(III) supramolecules has also increased with longer ^{3}MLCT excited state lifetimes. The $[\{(Ph_2phen)_2Ru(dpp)\}_2RhBr_2](PF_6)_5$ trimetallic complex has a significantly longer lived ^{3}MLCT excited state (τ = 40 ns) than $[\{(bpy)_2Ru(dpp)\}_2RhBr_2](PF_6)_5$ (τ = 26 ns) but $[\{(Ph_2phen)_2Ru(dpp\})_2RhBr_2](PF_6)_5$ produces more hydrogen (TOF = 31 h^{-1} for $[\{(Ph_2phen)_2Ru(dpp)\}_2RhBr_2](PF_6)_5$ and TOF = 27 h^{-1} for $[\{(bpy)_2Ru(dpp)\}_2RhBr_2](PF_6)_5$ in DMF).[7b,7c]

The rate constant for electron transfer (k_{et}) which determines τ when radiative and nonradiative decay rate constants are held constant, is most likely not the rate-determining step in photocatalysis. Intermolecular quenching of the ^{3}MLCT excited state by a sacrificial electron donor fills the electron hole on Ru.[7b] The k_{et} for $[\{(Ph_2phen)_2Ru(dpp)\}_2RhBr_2]^{5+}$ ($k_{et} = 2.0 \times 10^7$ s^{-1}) is less than that of $[\{(bpy)_2Ru(dpp)\}_2RhBr_2]^{5+}$ ($k_{et} = 2.3 \times 10^7$ s^{-1}).[7c,47] However, the longer ^{3}MLCT excited

state lifetime of $[\{(Ph_2phen)_2Ru(dpp)\}_2RhBr_2]^{5+}$ provides more time for intermolecular quenching. The excited state lifetime of $[(Ph_2phen)_2Ru(dpp)RhCl_2(dcmbpy)](PF_6)_3$ allows twice as much time for intermolecular quenching by the sacrificial electron donor than the lifetimes of $[(Ph_2phen)_2Ru(dpp)RhCl_2(Me_2bpy)](PF_6)_3$ and $[(Ph_2phen)_2Ru(dpp)RhCl_2(bpy)](PF_6)_3$. The extended lifetime resulting from carbomethoxy substitution produces significantly more hydrogen.

4. Conclusions and Future Work

4.1. Conclusions

Electron-withdrawing substitution of the terminal ligand on Rh with carbomethoxy substituents in these Ru(II), Rh(III) supramolecular complexes increases photocatalytic water reduction compared with complexes containing non-substituted or electron-donating substituted terminal ligands. $[(Ph_2phen)_2Ru(dpp)RhCl_2(dcmbpy)](PF_6)_3$ photocatalyzes water reduction with a 3.1 h^{-1} TOF compared with $[(Ph_2phen)_2Ru(dpp)RhCl_2(bpy)](PF_6)_3$ and $[(Ph_2phen)_2Ru(dpp)RhCl_2(Me_2bpy)](PF_6)_3$ which photocatalytically reduce water with a TOF of 1.8 h^{-1} and 1.5 h^{-1}, respectively, in the first 20 hours. The increased hydrogen production of $[(Ph_2phen)_2Ru(dpp)RhCl_2(dcmbpy)](PF_6)_3$ is likely due to a combination of the increased rate of chloride loss and longer ^{3}MLCT excited state lifetime. The electron-withdrawing substituent may stabilize the ^{3}MMCT excited state into the Marcus inverted region, but that cannot be determined within the scope of the current analysis.

The rate of chloride loss upon Rh reduction increases with electron-withdrawing substitution and correlates with enhanced water reduction. The rate constant for chloride loss upon $Rh^{III/II}$ reduction is 0.7 s^{-1} with the dcmbpy terminal ligand and 0.2 s^{-1} with Me_2bpy. Stabilization of Rh-based orbitals is unclear. The positive shift of the $E_{1/2}$ for the first and second reductions in $[(Ph_2phen)_2Ru(dpp)RhCl_2(dcmbpy)](PF_6)_3$ may be attributed to orbital stabilization, increased rate of halide loss, or both. Importantly, the rate at which the water substrate can interact with the catalytic Rh site increases as the chloride leaves more quickly.

The long-lived ^{3}MLCT excited state of $[(Ph_2phen)_2Ru(dpp)RhCl_2(dcmbpy)](PF_6)_3$ combined with the increased hydrogen production suggest that the rate-determining step

is intermolecular electron transfer from the sacrificial donor. The rate of hydrogen production should increase with increasing k_{et} and decrease with increasing τ if intramolecular electron transfer is the rate-determining step. The k_{et} in the carbomethoxy substituted complex is less than that in both the methyl and unsubstituted catalysts, assuming the k_r and k_{nr} are constant with a consistent light absorbing unit, but it photocatalyzes water reduction at an increased rate compared with the other two complexes. The concentration of $[(Ph_2phen)_2Ru(dpp)RhCl_2(dcmbpy)](PF_6)_3$ in the ^{3}MLCT excited state is higher than the ^{3}MLCT excited state concentration of the other two complexes at any given time because of the greater τ and thus has more opportunity for bimolecular quenching by the sacrificial donor.

It is assumed in the previous argument that radiative and non-radiative decay rate constants remain constant within the three complexes discussed because the light absorbing unit is held constant. Based on the differences in the τ, k_r and k_{nr} of $[Ru(deeb)_3]^{2+}$, it is possible that the radiative and non-radiative decay mechanisms of the ^{3}MLCT excited state of $[(Ph_2phen)_2Ru(dpp)RhCl_2(dcmbpy)](PF_6)_3$ is different from the 3MLCT excited state deactivation of $[(Ph_2phen)_2Ru(dpp)RhCl_2(bpy)](PF_6)_3$ and $[(Ph_2phen)_2Ru(dpp)RhCl_2(Me_2bpy)](PF_6)_3$. While the longer τ suggests stabilization of the ^{3}MMCT excited state into the Marcus inverted region, the τ of comparable molecules with other electron-withdrawing groups should be examined prior to concluding stabilization into the Marcus inverted region.

4.2. Future Work

A greater τ implies a lower k_r, k_{nr} or k_{et} (**eq. 1.5**). The cause of the long-lived τ of $[(Ph_2phen)_2Ru(dpp)RhCl_2(dcmbpy)](PF_6)_3$ is not quantified. Because of the difference in the ^{3}MLCT excited state energy among the three complexes, it cannot be assumed that the k_r and k_{nr} remain constant. The k_{et} of the complex with an electron-withdrawing substituent was expected to be greater than that of the other two complexes. The electrochemical data suggests possible stabilization of the unoccupied Rh orbitals, which coincides with ^{3}MMCT excited state stabilization. Investigation of the k_{et} with femtosecond transient absorption spectroscopy will provide more information about excited state behavior.

The results of this work indicate that electron-withdrawing substitution of the terminal ligand of Rh generates a better photocatalyst for water reduction. A more complete analysis should involve investigation of photocatalysis with other electron-withdrawing substituents. Synthesis and characterization of a molecule containing the terminal ligand 4,4′-bis(trifluoromethyl)-2,2′-bipyridine ($(CF_3)_2$bpy) would be useful to understanding possible stabilization of the ^{3}MMCT excited state into the Marcus inverted region. The CF_3 substituents are electron-withdrawing but do not greatly alter the τ, k_r or k_{nr} of $Ru((CF_3)_2bpy)_3]^{2+}$.[43] A more extensive series of molecules containing carboxy-substituted bipyridine and other electron-withdrawing groups would allow for a more thorough analysis of ^{3}MMCT excited state stabilization.

5. References

1. (a) Tsao, J.; Lewis, N.; Crabtree, G. *Basic Energy Needs in Solar Energy Utilization*; Sandia National Laboratory: Albuquerque, NM, 2006; (b) Conti, J. *International Energy Outlook*; Department of Energy/Energy Information Administration: Washington, DC, 2013.

2. (a) Karkas, M. D.; Verho, O.; Johnston, E. V.; Akermark, B., Artificial Photosynthesis: Molecular Systems for Catalytic Water Oxidation. *Chem. Rev.* **2014**; (b) Ardo, S.; Meyer, G. J., Photodriven Heterogeneous Charge Transfer with Transition-Metal Compounds Anchored to TiO2 Semiconductor Surfaces. *Chem. Soc. Rev.* **2009,** *38*, 115-164; (c) Concepcion, J. J.; Jurss, J. W.; Brennaman, M. K.; Hoertz, P. G.; Patrocinio, A. O. T.; Iha, N. Y. M.; Templeton, J. L.; Meyer, T. J., Making Oxygen with Ruthenium Complexes. *Acc. Chem. Res.* **2009,** *42*, 1954-1965; (d) Bard, A. J.; Fox, M. A., Artificial Photosynthesis - Solar Splitting of Water to Hydrogen and Oxygen. *Acc. Chem. Res.* **1995,** *28*, 141-145.

3. Adkins, J. *Standard Tables for Reference Solar Spectral Irradiances: Direct Normal and Hemispherical on 37° Tilted Surface*; G173-03; American Society for Testing and Materials: West Conshohocken, PA, 2012.

4. (a) Lehn, J. M.; Sauvage, J. P., Chemical Storage of Light Energy - Catalytic Generation of Hydrogen by Visible-Light or Sunlight - Irradiation of Neutral Aqueous-

Solutions. *New J. Chem.* **1977,** *1*, 449-451; (b) Kirch, M.; Lehn, J. M.; Sauvage, J. P., Hydrogen Generation by Visible-Light Irradiation of Aqueous-Solutions of Metal-Complexes - Approach to the Photo-Chemical Conversion and Storage of Solar-Energy. *Helv. Chim. Acta* **1979,** *62*, 1345-1384.

5. Balzani, V.; Scandola, F., *Supramolecular Photochemistry*. Ellis Horwood Limited: Chichester, West Sussex, England, 1991.

6. Balzani, V.; Bergamini, G.; Marchioni, F.; Ceroni, P., Ru(II)-Bipyridine Complexes in Supramolecular Systems, Devices and Machines. *Coord. Chem. Rev.* **2006,** *250*, 1254-1266.

7. (a) Elvington, M.; Brown, J.; Arachchige, S. M.; Brewer, K. J., Photocatalytic Hydrogen Production from Water Employing a Ru, Rh, Ru Molecular Device for Photoinitiated Electron Collection. *J. Am. Chem. Soc.* **2007,** *129*, 10644-10645; (b) Arachchige, S. M.; Brown, J. R.; Chang, E.; Jain, A.; Zigler, D. F.; Rangan, K.; Brewer, K. J., Design Considerations for a System for Photocatalytic Hydrogen Production from Water Employing Mixed-Metal Photochemical Molecular Devices for Photoinitiated Electron Collection. *Inorg. Chem.* **2009,** *48*, 1989-2000; (c) White, T. A.; Higgins, S. L. H.; Arachchige, S. M.; Brewer, K. J., Efficient Photocatalytic Hydrogen Production in a Single-Component System Using Ru,Rh,Ru Supramolecules Containing 4,7-Diphenyl-1,10-Phenanthroline. *Angew. Chem. Int. Ed.* **2011,** *50*, 12209-12213; (d) Wang, J.; White, T. A.; Arachchige, S. M.; Brewer, K. J., A new structural motif for photoinitiated electron collection: Ru,Rh bimetallics providing insight into H_2 production via photocatalysis of water reduction by Ru,Rh,Ru supramolecules. *Chem. Commun.* **2011,** *47*, 4451-4453; (e) Knoll, J. D.; Arachchige, S. M.; Brewer, K. J., A Structurally Diverse Ru-II, Pt-II Tetrametallic Motif for Photoinitiated Electron Collection and Photocatalytic Hydrogen Production. *ChemSusChem* **2011,** *4*, 252-261; (f) Zhou, R.; Sedai, B.; Manbeck, G. F.; Brewer, K. J., New Supramolecular Structural Motif Coupling a Ruthenium(II) Polyazine Light Absorber to a Rhodium(I) Center. *Inorg. Chem.* **2013,** *52*, 13314-13324; (g) White, T. A.; Mallalieu, H. E.; Wang, J.; Brewer, K. J., Mechanistic Insight into the Electronic Influences Imposed by Substituent Variation in Polyazine-Bridged Ruthenium(II)/Rhodium(III) Supramolecules. *Chem. Eur. J.* **2014,** *20*, 8265-8268; (h) White, T. A.; Whitaker, B. N.; Brewer, K. J., Discovering the Balance of Steric

and Electronic Factors Needed To Provide a New Structural Motif for Photocatalytic Hydrogen Production from Water. *J. Am. Chem. Soc.* **2011,** *133*, 15332-15334.

8. (a) Concepcion, J. J.; Jurss, J. W.; Brennaman, M. K.; Hoertz, P. G.; Patrocinio, A. O. T.; Murakami Iha, N. Y.; Templeton, J. L.; Meyer, T. J., Making Oxygen with Ruthenium Complexes. *Acc. Chem. Res.* **2009,** *42*, 1954-1965; (b) Campagna, S.; Puntoriero, F.; Nastasi, F.; Bergamini, G.; Balzani, V., Photochemistry and Photophysics of Coordination Compounds: Ruthenium. In *Photochemistry and Photophysics of Coordination Compounds I*, Balzani, V.; Campagna, S., Eds. 2007; Vol. 280, pp 117-214.

9. Kalyanasundaram, K., Photophysics, Photochemistry and Solar-Energy Conversion with Tris(Bipyridyl)Ruthenium(II) and its Analogs. *Coord. Chem. Rev.* **1982,** *46*, 159-244.

10. Lin, C. T.; Sutin, N., Steady-State Considerations in Electron-Transfer Quenching of Tris(2,2'-Bipyridine)Ruthenium(II) Luminescence. *J. Am. Chem. Soc.* **1975,** *97*, 3543-3545.

11. Rasmussen, S. C.; Richter, M. M.; Yi, E.; Place, H.; Brewer, K. J., Synthesis and Characterization of a Series of Novel Rhodium and Iridium Complexes Containing Polypyridyl Bridging Ligands - Potential Uses in the Development of Multimetal Catalysts for Carbon-Dioxide Reduction. *Inorg. Chem.* **1990,** *29*, 3926-3932.

12. Knoll, J. D.; Higgins, S. H.; White, T. A.; Brewer, K. J., Subunit Variation to Uncover Properties of Polyazine-Bridged Ru(II), Pt(II) Supramolecules with Low Lying Charge Separated States Providing Insight into the Functioning as H_2O Reduction Photocatalysts to Produce H_2. *Inorg. Chem.* **2013,** *52*, 9749-9760.

13. Amarante, D.; Cherian, C.; Ernmel, C.; Chen, H. Y.; Dayal, S.; Koshy, M.; Megehee, E. G., Improved Synthetic Routes to Rhodium Bipyridine Complexes: Comparison of Microwave vs. Conventional Synthesis. *Inorg. Chim. Acta* **2005,** *358*, 2231-2238.

14. Marcus, R. A., Electron-Transfer Reactions in Chemistry - Theory and Experiment. *Reviews of Modern Physics* **1993,** *65*, 599-610.

15. Ion Permeation and Chemical Kinetics. *The Journal of General Physiology* **1999,** *114*, 601-604.

16. Rangan, K.; Arachchige, S. M.; Brown, J. R.; Brewer, K. J., Solar Energy Conversion Using Photochemical Molecular Devices: Photocatalytic Hydrogen Production from Water Using Mixed-Metal Supramolecular Complexes. *Energy & Environmental Science* **2009,** *2*, 410-419.

17. Vlcek, A. A.; Dodsworth, E. S.; Pietro, W. J.; Lever, A. B. P., Excited State Redox Potentials of Ruthenium Diimine Complexes; Correlations with Ground State Redox Potentials and Ligand Parameters. *Inorg. Chem.* **1995,** *34*, 1906-1913.

18. Nicholson, R. S.; Shain, I., Theory of Stationary Electrode Polarography. Single Scan and Cyclic Methods Applied to Reversible, Irreversible, and Kinetic Systems. *Anal. Chem.* **1964,** *36*, 706-723.

19. Wang, J. The Design, Synthesis and Study of Mixed-Metal Ru,Rh and Os,Rh Complexes with Biologically Relevant Reactivity. Virginia Tech, Blacksburg, VA, 2012.

20. Huheey, J. A.; Keiter, E. A.; Keiter, R. L., *Inorganic Chemistry: Principles of Structure and Reactivity*. 4th Edition ed.; HarperCollins College Publishers: New York, NY, 1993.

21. (a) Kew, G.; Dearmond, K.; Hanck, K., Electrochemistry of Rhodium-Dipyridyl Complexes. *J. Phys. Chem.* **1974,** *78*, 727-734; (b) Kew, G.; Hanck, K.; Dearmond, K., Voltammetry of Rhodium-1,10-Phenanthroline Complexes. *J. Phys. Chem.* **1975,** *79*, 1828-1835.

22. (a) BorowiakResterna, A.; Szymanowski, J.; Voelkel, A., Structure and Nitrogen Basicity of Pyridine Metal Extractants. *Journal of Radioanalytical and Nuclear Chemistry-Articles* **1996,** *208*, 75-86; (b) Bansal, R. K., *Heterocyclic Chemistry*. 3rd ed.; New Age International Publishers: Daryaganj, New Delhi, 1999.

23. (a) Oki, A. R.; Morgan, R. J., An Efficient Preparation of 4,4'-Dicarboxy-2,2'-Bipyridine. *Synth. Commun.* **1995,** *25*, 4093-4097; (b) Gillaizeau-Gauthier, I.; Odobel, F.; Alebbi, M.; Argazzi, R.; Costa, E.; Bignozzi, C. A.; Qu, P.; Meyer, G. J., Phosphonate-Based Bipyridine Dyes for Stable Photovoltaic Devices. *Inorg. Chem.* **2001,** *40*, 6073-6079.

24. (a) Basile, L. A.; Barton, J. K., Design of a Double-Stranded DNA Cleaving Agent with 2 Polyamine Metal-Binding Arms - $Ru(dip)_2Macron^+$. *J. Am. Chem. Soc.* **1987,** *109*, 7548-7550; (b) Mongelli, M. T.; Brewer, K. J., Synthesis and Study of the

Light Absorbing, Redox and Photophysical Properties of Ru(II) and Os(II) Complexes of 4,7-Diphenyl-1,10-Phenanthroline Containing the Polyazine Bridging Ligand 2,3-bis(2-Pyridyl)Pyrazine. *Inorg. Chem. Commun.* **2006,** *9,* 877-881.

25. Zhou, R. New Polyazine-bridged Ru^{II},Rh^{III} and Ru^{II},Rh^{I} Supramolecular Photocatalysts for Water Reduction to Hydrogen Applicable for Solar Energy Conversion and Mechanistic Investigation of the Photocatalytic Cycle. Virginia Tech, Blacksburg, VA, 2014.

26. Bieda, R.; Ott, I.; Dobroschke, M.; Prokop, A.; Gust, R.; Sheldrick, W. S., Structure-Activity Relationships and DNA Binding Properties of Apoptosis Inducing Cytotoxic Rhodium(III) Polypyridyl Complexes Containing the Cyclic Thioether[9]aneS(3). *J. Inorg. Biochem.* **2009,** *103,* 698-708.

27. Zigler, D. F.; Wang, J.; Brewer, K. J., Ruthenium(II)-Polyazine Light Absorbers Bridged to Reactive cis-Dichlororhodium(III) Centers in a Bimetallic Molecular Architecture. *Inorg. Chem.* **2008,** *47,* 11342-11350.

28. (a) Caspar, J. V.; Kober, E. M.; Sullivan, B. P.; Meyer, T. J., Application of the Energy-Gap Law to the Decay of Charge-Transfer Excited States. *J. Am. Chem. Soc.* **1982,** *104,* 630-632; (b) Stoll, T.; Gennari, M.; Serrano, I.; Fortage, J.; Chauvin, J.; Odobel, F.; Rebarz, M.; Poizat, O.; Sliwa, M.; Deronzier, A.; Collomb, M.-N., $[Rh^{III}(dmbpy)_2Cl_2]^+$ as a Highly Efficient Catalyst for Visible-Light-Driven Hydrogen Production in Pure Water: Comparison with Other Rhodium Catalysts. *Chemistry-a European Journal* **2013,** *19,* 781-791.

29. Stoll, T.; Gennari, M.; Fortage, J.; Castillo, C. E.; Rebarz, M.; Sliwa, M.; Poizat, O.; Odobel, F.; Deronzier, A.; Collomb, M.-N., An Efficient Ru-II-Rh-III-Ru-II Polypyridyl Photocatalyst for Visible-Light-Driven Hydrogen Production in Aqueous Solution. *Angewandte Chemie-International Edition* **2014,** *53,* 1654-1658.

30. Kalyanasundaram, K., *Photochemistry of Polypyridine and Porphyrin Complexes*. Academic Press: San Diego, CA, 1992.

31. Xie, J.; Li, C.; Zhou, Q.; Wang, W.; Hou, Y.; Zhang, B.; Wang, X., Large Improvement in the Catalytic Activity Due to Small Changes in the Diimine Ligands: New Mechanistic Insight into the Dirhodium(II,II) Complex-Based Photocatalytic H_2 Production. *Inorg. Chem.* **2012,** *51,* 6376-6384.

32. (a) Balzani, V.; Juris, A.; Venturi, M.; Campagna, S.; Serroni, S., Luminescent and Redox-Active Polynuclear Transition Metal Complexes. *Chem. Rev.* **1996,** *96*, 759-833; (b) Indelli, M. T.; Bignozzi, C. A.; Harriman, A.; Schoonover, J. R.; Scandola, F., 4 Intercomponent Processes in a Ru(II)-Rh(III) Polypyridine Dyad - Electron-Transfer from Excited Donor, Electron-Transfer to Excited Acceptor, Charge Recombination, and Electronic-Energy Transfer. *J. Am. Chem. Soc.* **1994,** *116*, 3768-3779; (c) Indelli, M. T.; Scandola, F.; Collin, J. P.; Sauvage, J. P.; Sour, A., Photoinduced Electron and Energy Transfer in Rigidly Bridged Ru(II)-Rh(III) Binuclear Complexes. *Inorg. Chem.* **1996,** *35*, 303-312; (d) Maity, D.; Bhaumik, C.; Karmakar, S.; Baitalik, S., Photoinduced Electron and Energy Transfer and pH-Induced Modulation of the Photophysical Properties in Homo- and Heterobimetallic Complexes of Ruthenium(II) and Rhodium(III) Based on a Heteroditopic Phenanthroline-Terpyridine Bridge. *Inorg. Chem.* **2013,** *52*, 7933-7946; (e) Macqueen, D. B.; Petersen, J. D., Competitive Hydrogen-Production and Emission Through the Photochemistry of Mixed-Metal Bimetallic Complexes. *Inorg. Chem.* **1990,** *29*, 2313-2320; (f) Nozaki, K.; Ohno, T.; Haga, M., Intramolecular Electron-Transfer in Photoexcited Ru(II)-Rh(III) Binuclear Compounds. *J. Phys. Chem.* **1992,** *96*, 10880-10888; (g) van Diemen, J. H.; Hage, R.; Haasnoot, J. G.; Lempers, H. E. B.; Reedijk, J.; Vos, J. G.; Decola, L.; Barigelletti, F.; Balzani, V., Electrochemical and Photophysical Properties of New Triazole-Bridged Heterobimetallic Ruthenium Rhodium and Ruthenium Iridium Complexes. *Inorg. Chem.* **1992,** *31*, 3518-3522.

33. Rogers, H. M.; White, T. A.; Stone, B. N.; Arachchige, S. M.; Brewer, K. J., Nonchromophoric Halide Ligand Variation in Polyazine-Bridged Ru(II),Rh(III) Bimetallic Supramolecules Offering New Insight into Photocatalytic Hydrogen Production from Water. *Inorg. Chem.* **2015,** *54*, 3545-3551.

34. Bard, A. J.; Faulkner, L. R., *Electrochemical Methods: Fundamentals and Applications*. 2nd Edition ed.; John Wiley & Sons, Inc.: Hoboken, NJ, 2001.

35. Steckhan, E.; Herrmann, S.; Ruppert, R.; Dietz, E.; Frede, M.; Spika, E., Analytical Study of a Series of Substituted (2,2'-Bipyridyl)(Pentamethylcyclopentadienyl)Rhodium and Iridium Complexes with Regard to Their Effectiveness as Redox Catalysts for the Indirect Electrochemical and Chemical-Reduction of $NAD(P)^+$. *Organometallics* **1991,** *10*, 1568-1577.

36. Hildebrand, F.; Kohlmann, C.; Franz, A.; Luetz, S., Synthesis, Characterization and Application of New Rhodium Complexes for Indirect Electrochemical Cofactor Regeneration. *Adv. Synth. Catal.* **2008,** *350*, 909-918.

37. Creutz, C.; Keller, A. D.; Sutin, N.; Zipp, A. P., Poly(Pyridine)Ruthenium(II)-Photoinduced Redox Reactions of Bipyridinium Cations, Poly(Pyridine)Rhodium Complexes, and Osmium Ammines. *J. Am. Chem. Soc.* **1982,** *104*, 3618-3627.

38. (a) Wang, J.; White, T. A.; Arachchige, S. M.; Brewer, K. J., A new structural motif for photoinitiated electron collection: Ru,Rh bimetallics providing insight into H-2 production via photocatalysis of water reduction by Ru,Rh,Ru supramolecules. *Chem. Commun.* **2011,** *47*, 4451-4453; (b) Kalyanasundaram, K.; Gratzel, M.; Nazeeruddin, M. K., Excited-State Interactions in Ligand-Bridged Chromophore Quencher Complexes Containing Rhodium(III) and Ruthenium(II) Polypyridyl Units. *J. Phys. Chem.* **1992,** *96*, 5865-5872; (c) Ortmans, I.; Didier, P.; Kirschdemesmaeker, A., New Charge-Transfer Luminescent Polymetallic Complexes of Rhodium(III), Iridium(III), and Ruthenium(II) with the Bridging Ligand 1,4,5,8,9,12-Hexaazatriphenylene. *Inorg. Chem.* **1995,** *34*, 3695-3704.

39. Juris, A.; Balzani, V.; Barigelletti, F.; Campagna, S.; Belser, P.; Vonzelewsky, A., Ru(II) Polypyridine Complexes - Photophysics, Photochemistry, Electrochemistry and Chemi-Luminescence. *Coord. Chem. Rev.* **1988,** *84*, 85-277.

40. (a) Englman, R.; Jortner, J., Energy Gap Law for Radiationless Transitions in Large Molecules. *Mol. Phys.* **1970,** *18*, 145-&; (b) Caspar, J. V.; Kober, E. M.; Sullivan, B. P.; Meyer, T. J., Application of the Energy-Gap Law to the Decay of Charge-Transfer Excoted-States. *J. Am. Chem. Soc.* **1982,** *104*, 630-632; (c) Caspar, J. V.; Meyer, T. J., Application of the Energy-Gap Law to Nonradiative, Excited-State Decay. *J. Phys. Chem.* **1983,** *87*, 952-957.

41. Barbante, G. J.; Hogan, C. F.; Wilson, D. J. D.; Lewcenko, N. A.; Pfeffer, F. M.; Barnett, N. W.; Francis, P. S., Simultaneous Control of Spectroscopic and Electrochemical Properties in Functionalised Electrochemiluminescent Tris(2,2 '-Bipyridine)Ruthenium(II) Complexes. *Analyst* **2011,** *136*, 1329-1338.

42. Cook, M. J.; Lewis, A. P.; McAuliffe, G. S. G.; Skarda, V.; Thomson, A. J.; Glasper, J. L.; Robbins, D. J., Luminescent Metal-Complexes. Part 1. Tris-Chelates of

Substituted 2,2'-Bipyridyls with Ruthenium(II) As Dyes For Luminescent Solar Collectors. *Journal of the Chemical Society-Perkin Transactions 2* **1984**, 1293-1301.

43. Cook, M. J.; Lewis, A. P.; McAuliffe, G. S. G.; Skarda, V.; Thomson, A. J.; Glasper, J. L.; Robbins, D. J., Luminescent Metal-Complexes. 2. A Model for the Luminescence Properties of the Tris-Chelates of Substituted 2,2'-Bipyridyls with Ruthenium(II). *Journal of the Chemical Society-Perkin Transactions 2* **1984**, 1303-1307.

44. Kalyanasundaram, K.; Nazeeruddin, M. K.; Gratzel, M.; Viscardi, G.; Savarino, P.; Barni, E., Synthesis and Photophysical Characterization of Highly Luminescent Complexes of Ru(IIO) Containing 4,4'-Di-(para-carboxyphenyl)-2,2'-bipyridine. *Inorg. Chim. Acta* **1992,** *198*, 831-839.

45. Maeda, K.; Sahara, G.; Eguchi, M.; Ishitani, O., Hybrids of a Ruthenium(II) Polypyridyl Complex and a Metal Oxide Nanosheet for Dye-Sensitized Hydrogen Evolution with Visible Light: Effects of the Energy Structure on Photocatalytic Activity. *Acs Catalysis* **2015,** *5*, 1700-1707.

46. Tong, L.; Zong, R.; Thummel, R. P., Visible Light-Driven Hydrogen Evolution from Water Catalyzed by A Molecular Cobalt Complex. *J. Am. Chem. Soc.* **2014,** *136*, 4881-4884.

47. White, T. A.; Arachchige, S. M.; Sedai, B.; Brewer, K. J., Emission Spectroscopy as a Probe into Photoinduced Intramolecular Electron Transfer in Polyazine Bridged Ru(II),Rh(III) Supramolecular Complexes. *Materials* **2010,** *3*, 4328-4354.

6. Appendix

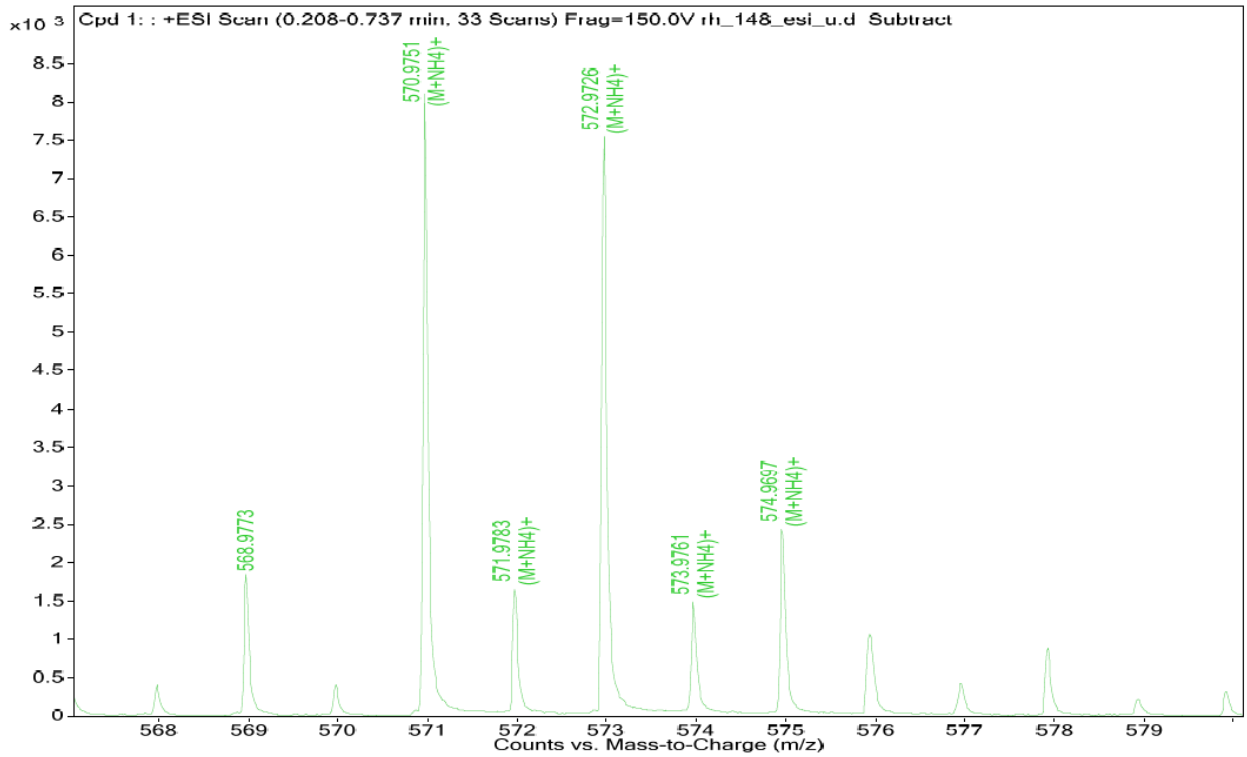

Figure A.1: Mass spectrum molecular ion peak of (dcmbpy)$RhCl_3$·DMF.

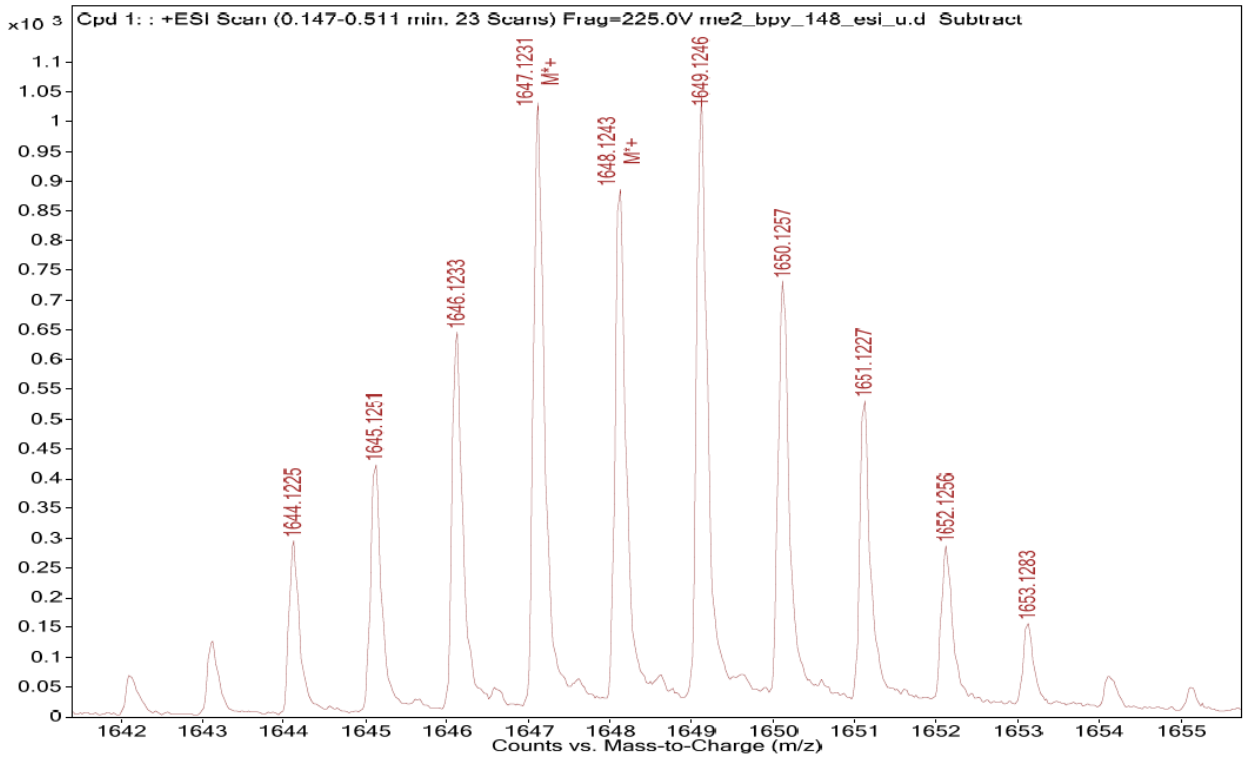

Figure A.2: Mass spectrum of $[(Ph_2phen)_2Ru(dpp)RhCl_2(Me_2bpy)](PF_6)_3$. Molecular ion peak is $[[(Ph_2phen)_2Ru(dpp)RhCl_2(Me_2bpy)](PF_6)_2]^+$.

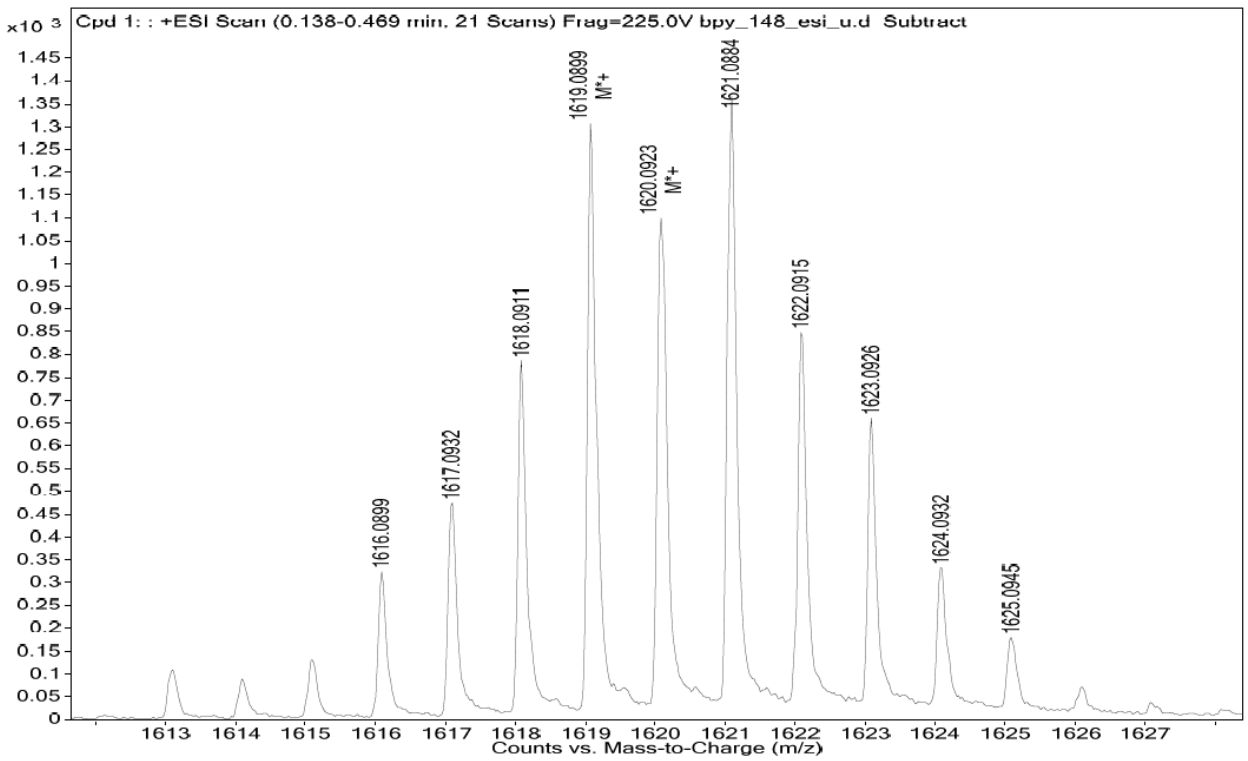

Figure A.3: Mass spectrum of $[(Ph_2phen)_2Ru(dpp)RhCl_2(bpy)](PF_6)_3$. Molecular ion peak is $[[(Ph_2phen)_2Ru(dpp)RhCl_2(bpy)](PF_6)_2]^+$.

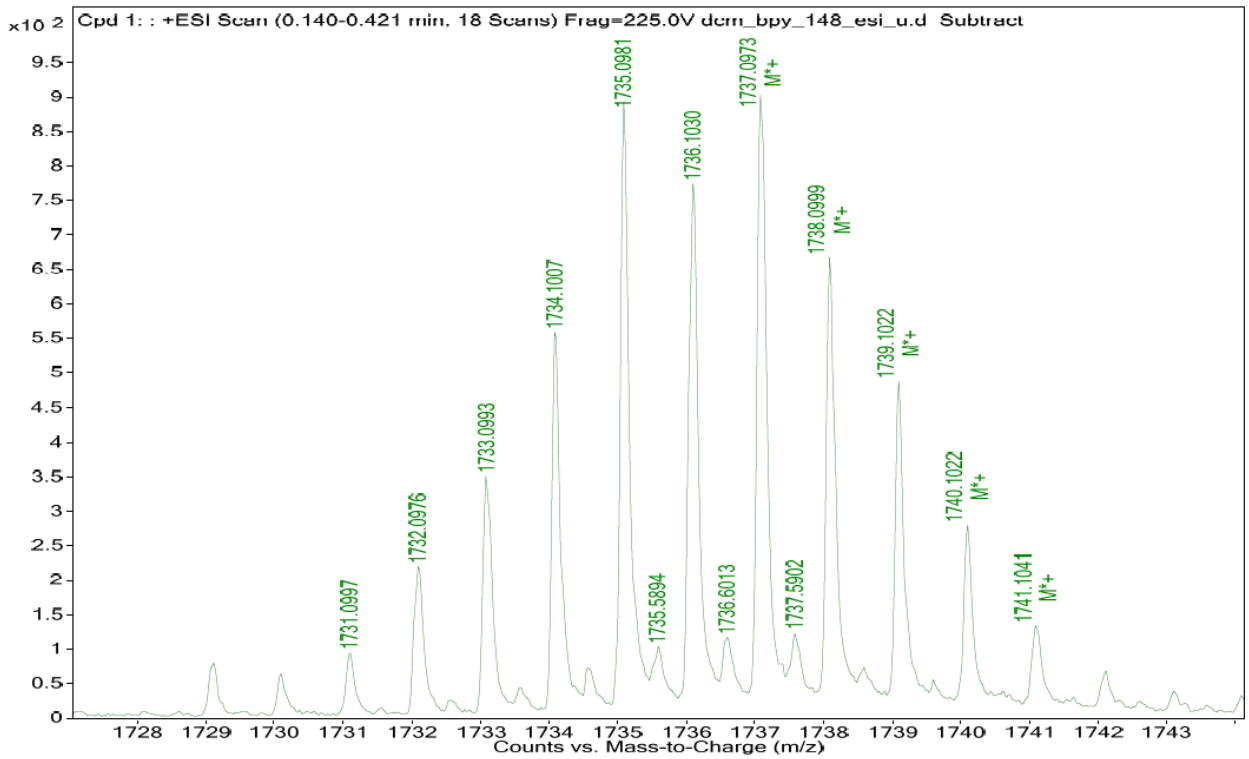

Figure A.4: Mass spectrum of $[(Ph_2phen)_2Ru(dpp)RhCl_2(dcmbpy)](PF_6)_3$. Molecular ion peak is $[[(Ph_2phen)_2Ru(dpp)RhCl_2(dcmbpy)](PF_6)_2]^+$.

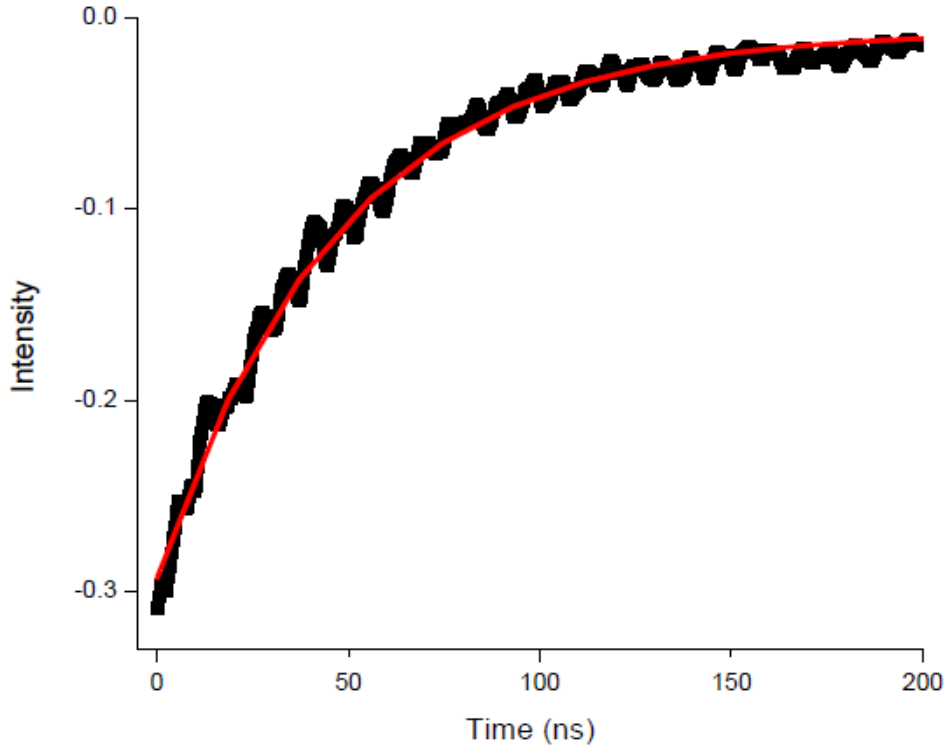

Figure A.5: Excited state decay plot for $[(Ph_2phen)_2Ru(dpp)RhCl_2(Me_2bpy)](PF_6)_3$ in deaerated acetonitrile.

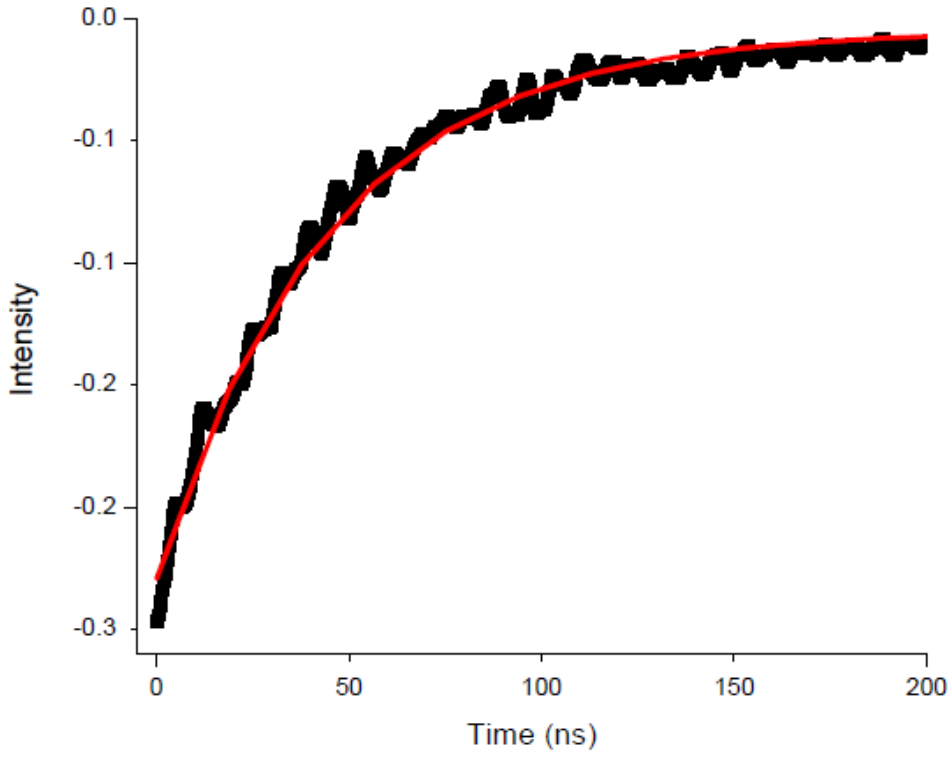

Figure A.6: Excited state decay plot for $[(Ph_2phen)_2Ru(dpp)RhCl_2(bpy)](PF_6)_3$ in deaerated acetonitrile.

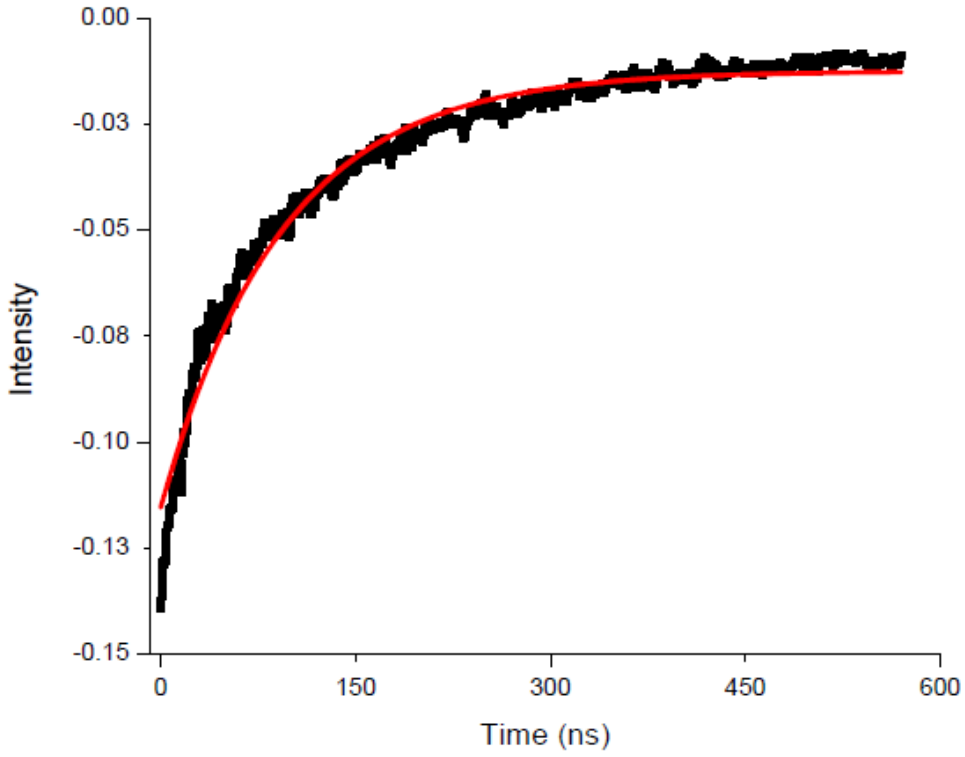

Figure A.7: Excited state decay plot for $[(Ph_2phen)_2Ru(dpp)RhCl_2(dcmbpy)](PF_6)_3$ in deaerated acetonitrile.